SC5508.FR

Copy No. 35

ENVIRONMENTAL INTEGRITY OF COATING/METAL INTERFACE

FINAL REPORT FOR THE PERIOD
March 1, 1987 through January 31, 1990

CONTRACT NO. N00014-87-C-0075

Prepared for

Scientific Officer
Metallic Materials Division, Code 1131M
Office of Naval Research
Arlington, VA 22217
Attn: Dr. A. John Sedriks

M. Kendig, Program Manager
and
R. Addison, J. Lumsden, P. Stocker, S. Jeanjaquet and D. Anderson

APRIL 1990

Approved for public release; distribution unlimited

Rockwell International
Science Center

UNCLASSIFIED

SECURITY CLASSIFICATION OF THIS PAGE

REPORT DOCUMENTATION PAGE

FORM APPROVED
OMB No. 0704-0188

1a. REPORT SECURITY CLASSIFICATION
UNCLASSIFIED

1b. RESTRICTIVE MARKINGS

2a. SECURITY CLASSIFICATION AUTHORITY

3. DISTRIBUTION/AVAILABILITY OF REPORT
Approved for public release; distribution is unlimited

2b. CLASSIFICATION/DOWNGRADING SCHEDULE

4. PERFORMING ORGANIZATION REPORT NUMBER(S)
SC5508.FR

5. MONITORING ORGANIZATION REPORT NUMBER(S)

6a. NAME OF PERFORMING ORGANIZATION
ROCKWELL INTERNATIONAL
Science Center

6b. OFFICE SYMBOL *(If Applicable)*

7a. NAME OF MONITORING ORGANIZATION

6c. ADDRESS *(City, State, and ZIP Code)*
1049 Camino Dos Rios
Thousand Oaks, CA 91360

7b. ADDRESS *(City, State and ZIP Code)*

8a. NAME OF FUNDING/SPONSORING ORGANIZATION
Scientific Officer
Metallic Materials Division

8b. OFFICE SYMBOL *(If Applicable)*

9. PROCUREMENT INSTRUMENT IDENTIFICATION NUMBER
CONTRACT NO. N00014-87-C-0075

8c. ADDRESS *(City, State and ZIP Code)*
Office of Naval Research
800 North Quincy Street
Arlington, VA 22217-5000

10. SOURCE OF FUNDING NOS.

PROGRAM ELEMENT NO.	PROJECT NO.	TASK NO.	WORK UNIT ACCESSION NO.

11. TITLE *(Include Security Classification)*
ENVIRONMENTAL INTEGRITY OF COATING/METAL INTERFACE

12. PERSONAL AUTHOR(S)
Kendig, M., Addison, R., Lumsden, J., Stocker, P., Jeanjaquet, S., and Anderson, D.

13a. TYPE OF REPORT	13b. TIME COVERED	14. DATE OF REPORT *(Year, Month, Day)*	15. PAGE COUNT
Final Report	FROM 03/01/87 TO 01/31/90	**1990, APRIL**	

16. SUPPLEMENTARY NOTATION

17 COSATI CODES			18. SUBJECT TERMS *(Continue on reverse if necessary and identify by block number)*
FIELD	GROUP	SUB-GROUP	

19. ABSTRACT *(Continue on reverse if necessary and identify by block number)*

The role of chemical and electrochemical reactions at the coating/metal interface in the region of a cathodic disbond in degrading adhesion of organic coatings to steel has been studied using scanning acoustic microscopy, wetting analysis and x-ray photo-electron spectroscopy (XPS). The results show that cathodic polarization accelerates adhesion loss by the combined effects of a shift in the zeta potential of the steel substrate and build-up of an alkaline sodium hydroxide electrolyte that chemically degrades the polymer. Cathodic formation of sodium hydroxide not only degrades the polymer, but also lowers the surface tension of the electrolyte so as to favor displacement of the polymer. A mechanism of interfacial bond rupture made irreversible by polymer degradation is proposed.

CONTINUED

20. DISTRIBUTION/AVAILABILITY OF ABSTRACT
UNCLASSIFIED/UNLIMITED ☐ SAME AS RPT. ☒ DTIC USERS ☐

21. ABSTRACT SECURITY CLASSIFICATION
UNCLASSIFIED

22a. NAME OF RESPONSIBLE INDIVIDUAL	22b. TELEPHONE NUMBER *(Include Area Code)*	22c. OFFICE SYMBOL
Dr. A. John Sedriks		**Code 1131M**

DD FORM 1473, JUN 86 **Previous editions are obsolete.**

UNCLASSIFIED

SECURITY CLASSIFICATION OF THIS PAGE

19. ABSTRACT (Cont'd)

Steel wettability was used as a probe of polymer adsorption in a series of experiments aimed at evaluating the acid/base behavior of the polymer metal interaction. Results suggest that the steel acts as a base in the Drago sense to the substrate acid. Therefore, an alkaline corrosion product competes effectively for the substrate. The surface of the steel substrate under cathodic disbond conditions is composed of Fe_3O_4 which remains stable over a broad potential range from −400 mV to −1030 mV (SCE). For potentials of −950 mV (SCE) and above the oxide is slightly oxidized. Below −1100 mV the oxide begins to reduce the metallic state. Wetting experiments suggest that improvement of the resistance to cathodic disbonding might be achieved by the incorporation of fixed positive charges in the polymer network.

Accesion For	
NTIS CRA&I	☑
DTIC TAB	☐
Unannounced	☐
Justification	
By	
Distribution /	
Availability Codes	
Dist	Avail and / or Special
A-1	

TABLE OF CONTENTS

LIST OF TABLES

LIST OF FIGURES

LIST OF FIGURES (Continued)

LIST OF FIGURES (Continued)

1.0 INTRODUCTION

Organic coatings provide one of the most cost effective means for corrosion protection of structural alloys and are used extensively in both commercial and military applications. Anticipated changes in coating technology brought about by environmental concerns for excessive volatile organic content (VOC) of paints will require rapid assessment of coatings to replace environmentally hazardous systems. Simplifying coating processes by eliminating surface conversion layers now required for adhesion of paints to steel would provide a benefit to manufacturing and structural maintenance. A critical need exists, therefore, for pinpointing the chemical and molecular events which limit the life of organic coatings on steel in a corrosive environment.

The focus of the work undertaken in this program has been on the role of the corrosive environment in degrading the adhesion of organic coatings on steel. Although the barrier nature of organic coatings plays a role in protecting the steel substrate, it must be recognized that adhesion and molecular blocking of active sites on the surface are crucial for providing corrosion resistance, and may actually determine the ultimate life of the coating system. In a recent review Walter stated: "The concept of the paint film as an impermeable membrane has been largely discredited by permeability data for water and oxygen".[1] This reflects earlier speculation by Gerhart that: "In principle, a perfectly 'glued' surface coating can be reasoned as the ultimate protectant, provided and if adhesion is perfect and enduring even allowing for absorbance and transport of nature's corrodents."[2] Clearly, adhesion or maintenance of an intimate molecular contact between a low dielectric constant, non-conducting organic material and a metal substrate diminishes the rate of corrosion of the metal despite the apparent facility of corrodents such as oxygen and ionic solutes to permeate the organic matrix. It is the objective of this project to understand the corrosion-induced degradation of adhesion of organic coating/metal systems. Understanding the fundamentals of corrosion-induced adhesion loss will lead to concepts for improving the resistance of the polymer/steel interface to corrosive degradation perhaps in the absence of the now necessary conversion coatings.

Figure 1[3] shows a schematic for the degradation of a polymer-coated metal interface on a metal having an oxide that is less dense than the metal substrate. According to this model, corrosion initiates at sites of initially present defects which are

anodically active relative to the portion of the metal covered by non-defective coating. The active metal at the defect anodically dissolves to form oxide corrosion products while driving the adjacent surface covered by electrolyte saturated coating cathodic. The cathodic polarization in the adjacent region alters the zeta potential (surface charge) of the substrate, reduces the metal oxide, and reduces oxygen and water to form a region of high alkalinity. These cathodic processes destroy adhesion of the organic film to the substrate and propagate the corrosion. It is, therefore, this cathodic process which determines the rate of failure of organic coatings on steel. Although it is more or less agreed that the cathodic reaction adversely influences the adhesion of organic coatings on steel to cause disbonding, the precise mechanism for the disbonding is not well established. Four types of mechanisms have been proposed in the recent literature, the first three of which have been summarized by Castle and Watts.[4] These mechanisms are:

1. Coating degradation[5-8]

2. Interfacial failure[9]

3. Dissolution of the substrate oxide[10]

4. Development of a weak fluid boundry layer[11]

It is most likely however that a mixed mode of attack occurs.

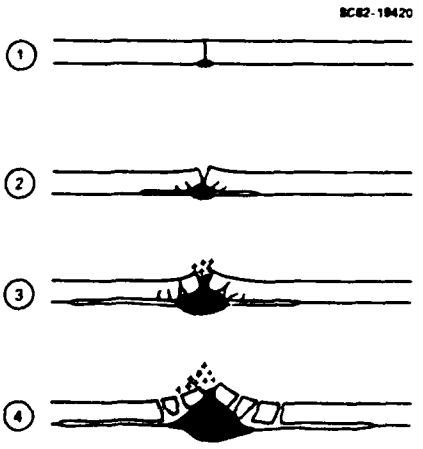

Fig. 1

Schematic for organic coating degradation by corrosion in aerated, neutral aqueous media.

2.0 OBJECTIVES

Based on the above considerations, experiments have been designed to:

1. Evaluate the kinetics of cathodic disbonding and the nature of the irreversible alkaline attack on a model organic coating.

2. Determine the role of the substrate chemistry on the disbonding process as it changes under cathodic polarization.

3. Determine the role of electrochemical potential and surface energetics on the preference of metallic surfaces for an aqueous electrolyte over an organic film.

3.0 SUMMARY OF RESULTS

Scanning acoustic microscopic evaluation of the disbonding process has been completed. The results have not only provided quantitative information on the disbonding process in terms of rate constants for steel as a function of surface chemistry, but have demonstrated the importance of the alkaline product from the cathodic reaction in degrading the polymer and advancing the disbond region.

A series of wetting experiments have been completed. These experiments have probed the acid-base nature of the steel/polymer adhesion. In one series of experiments the extent of polymer adsorption from various solvents was determined from the resulting hydrophobic behavior of the steel sample. This allowed determination of the relative acid/base interaction of steel with organic polymers. The approach is based on Fowkes adaptation of Drago acid/base scale for polymer adsorption. Results indicate that the steel surface formed under oxidizing conditions is more acidic than $CHCl_3$.

The advancing adhesion tension of steel for a pH 9.6 borate electrolyte contacting steel shows an irreversible increase with cathodic polarization. This has been attributed to electrochemically generated base which catalyzes the advance of aqueous contact to a rough surface.

Displacement of an absorbed polymer contained in a film of polymer solution from a steel surface modeled coating disbonding. The displacement of the polymer depends on the potential of zero charge of the steel as determined from capacitance evaluation. The polymer desorbs at potentials cathodic to the potential of zero charge (pzc), where displacement of the polymer-containing organic phase from steel by an aqueous phase occurs more easily. Incorporation of a positively charged organic ion in the organic phase inhibits the displacement of the organic film and suggests a possible structure for incorporation into polymer coatings to improve resistance to cathodic disbonding.

A number of experiments using the Science Center's pre-UHV sample preparation cell were made to elucidate the surface chemistry of iron under cathodic disbond conditions. The iron surface for potentials between -400 and -1100 mV vs SCE appears to be Fe_3O_4. For potentials more negative than -1100 mV (SCE) the iron oxide begins to disappear via electrochemical reduction to form the zero valent metal. For potentials

above -260 mV (SCE) iron(III) oxides are detected on the surface. The experiment was complicated by silica contamination from the preparation cell.

4.0 SUMMARY OF PREVIOUS RESULTS

4.1 Scanning Acoustic Microscopy[12-17]

A scanning acoustic microscope (SAM) used in conjunction with an in situ, three electrode electrochemical cell (Fig. 2) allowed rapid and accurate determination of the rate of cathodic disbonding of a thin (4 μm) hydroxy-terminated polybutadiene film (Polybd) from steel surfaces. Acoustic microscopy images changes in the acoustic properties of the solid-solid interface and changes in the mechanical properties of the polymer coating on steel. Such sensitivity is unavailable to conventional light-optical microscopy. These particular sensitivities and the in situ capability has allowed the disbonding process to be directly followed and quantified. Figure 3 shows time sequential acoustic micrographs taken for regions adjacent to a scribe in a Polybd coating on a polished and degreased (P+D) steel Q-panel. The specimen was polarized to -850 mV vs Ag/AgCl in the 0.5 M NaCl electrolyte. As can be seen a region containing a distribution of circular features grows away from the scribe (located at the bottom of the micrographs in Fig. 3). This region is associated with the cathodic disbonding as determined by a post test-tape pull. The circular features are attributed to the localized attack of the organic film by the cathodically generated alkali. Experiments showed that short time exposure of the coating to NaOH dramatically altered its acoustic impedance before significant change in light optical properties were observed. The extension of the region, d, away from the scribe could accurately be determined from the micrograph and determined as a function of time as shown in Fig. 4a. The disbond distance d for Polybd coated steel held in the 0.5 M NaCl at different potentials depends on time, t, as

$$d = d_o + K_d \sqrt{t} \qquad (1)$$

This time dependence is consistent with that observed by Leidheiser and Wang[18] and with the model proposed by Thornton.[11] The parabolic rate constant K_d depends on potential as show in Fig. 4b illustrating the increase in disbonding kinetics for cathodic polarization to potentials more negative than -700 mV vs Ag/AgCl.

Figure 4c shows that the cathodic build-up of an alkaline product alone propagates the disbonding even in the absence of polarization. Accordingly, d continues to

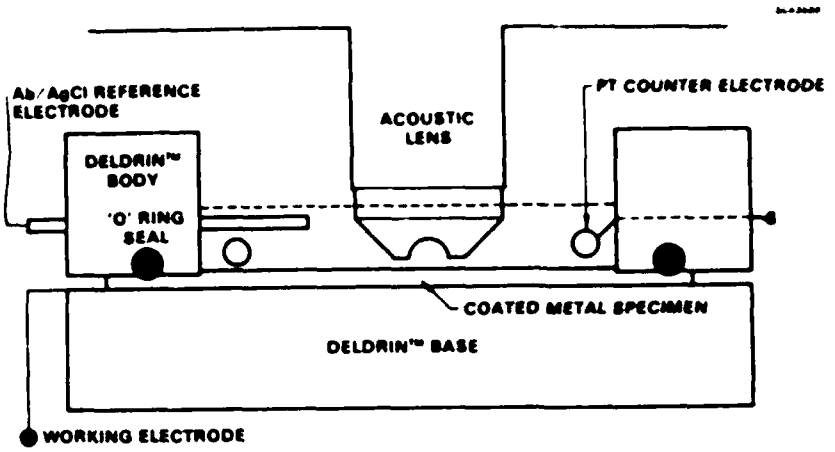

Fig. 2 Schematic for the in situ scanning acoustic microscopy (SAM) cell.

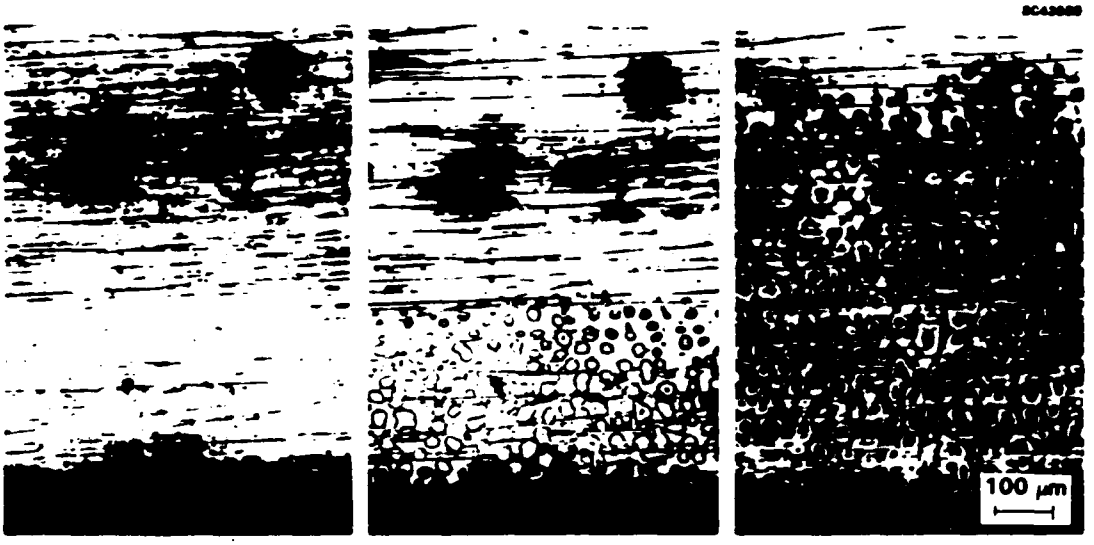

Fig. 3 SAM of hydroxy-terminated polybutadiene (Polybd) coated carbon steel (Q-panels) after 1.5 min., 35.3 min. and 100.3 min of cathodic polarization at -850 mV (Ag/AgCl).

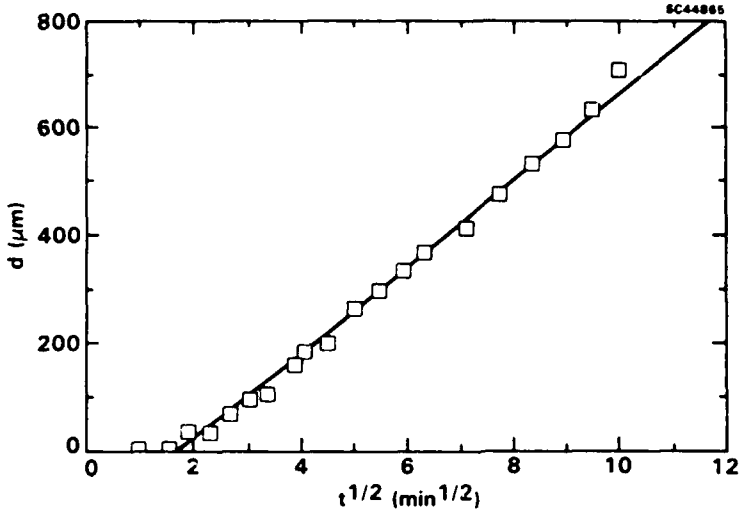

HYDROXY-TERMINATED POLYBUTADIENE
STEEL SUBSTRATE – 600 GRIT POLISHED AND DEGREASED
ELECTROLYTE– 0.5 M NaCl
POLARZED TO -850 mV vs Ag/AgCl

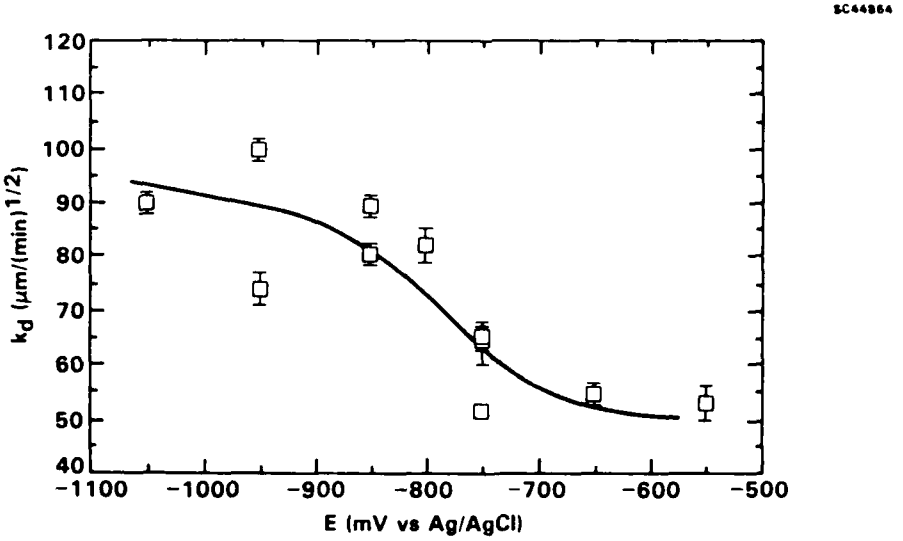

HYDROXY-TERMINATED POLYBUTADIENE
STEEL SUBSTRATE – 600 GRIT POLISHED AND DEGREASED
ELECTROLYTE – 0.5 M NaCl

Fig. 4 (a) Disbond distance from the scribe, d, vs the square root of time. (b) Disbonding parabolic rate constant, K_d, vs potential.

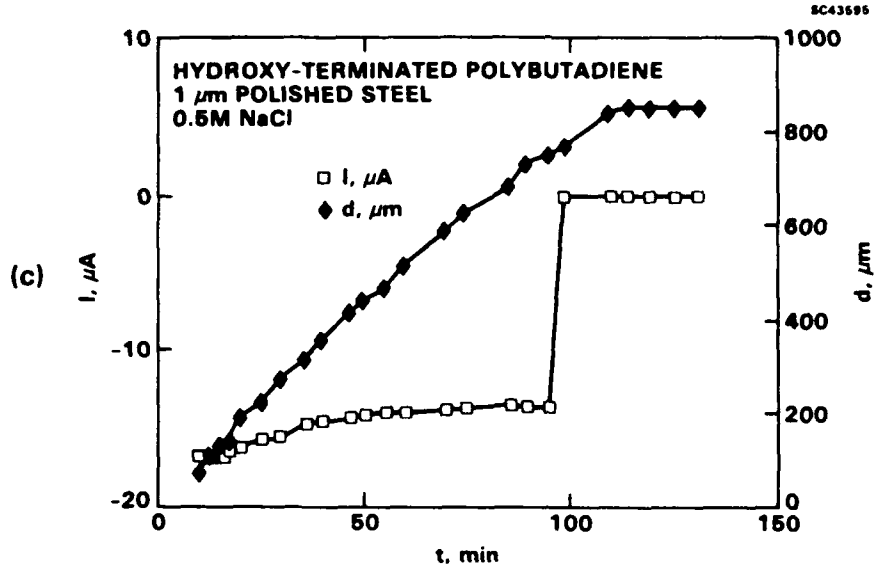

Fig. 4 (c) Time dependence for the current and d for a 1 μm polished and hydroxy-terminated polybutadiene-coated steel Q-panel.

increase for about 10 min after termination of the cathodic polarization (ca. 95 min in Fig. 4c). Eventually d becomes constant with time as the alkaline build-up dissipates in the absence of cathodic polarization (Fig. 4c).

The nature of the oxide/coating interphase also influences the disbonding process. Cathodic disbonding kinetics were obtained for different surface treatments. The results in terms of K_d Eq. (1) appear in Table 1. Uncertainty in K_d is expressed as ± one standard deviation determined by least squares fitting of the observations to Eq. (1). τ is an initiation time required before disbonding commences[§]. A highly polished surface pretreatment exhibits accelerated disbonding as compared to the standard polished (600 grit) and degreased (P+D) specimen. The initiation time for this specimen, however, is somewhat longer as compared to that for the P+D specimen (Table 1). The increase in K_d for the highly polished specimen may be attributed to the shorter, less tortuous diffusion path for the electrolyte along the disbond away from the scribe. The nitric acid treated specimen has a longer initiation time, and exhibits a lower disbond

§$\tau_o = (d_o/K_2)^2$.

rate as compared to the P+D specimen, K_d. The sample having a surface treated with the organo-titanate adhesion promoters (LICA #38) had half the disbond rate and a longer τ_o as compared to the P+D specimen (Table 1).

Table 1

K_d and τ Determined for a Polarization of -850 mV vs Ag/AgCl as a Function of Surface Preparation

Specimen ID	Specimen/Surface Treatment*	K_d ($\mu m/\sqrt{min}$)	τ_o (min)
65	P+D	82 ± 3	4
96	Polished < 1 μm	108 ± 4	25
53	P+D/HNO_3	68 ± 2	71
41	P+D/INH. HCl	52 ± 2	26
45	P+D/LICA in polymer	52 ± 1	2
46	P+D/LICA on surface	41 ± 2	27

*Glossary of Terms

P+D	Polished and degreased
HNO_3	Steel oxidized with HNO_3
INH.HCl	Steel cleaned with HCl containing inhibitor
LICA	Kenrich organotitanate coupling agent #38

4.2 Surface Analysis

In order to characterize the surface chemistry of steel under the conditions of cathodic polarization and high alkalinity , tests were initiated using the pre-UHV sample preparation cell shown in Fig. 5. This system allowed conditioning of test surfaces with respect to potential and electrolyte chemistry followed by a direct transfer into the UHV chamber for analysis by Auger electron spectroscopy (AES) or X-ray electron spectroscopy (XPS) without exposure to the laboratory environment. This is particularly important for exploring the nature of surface films on iron which exist for the reducing chemical and electrochemical conditions as existing in the cathodic disbond zone. Previously the system shown in Fig. 5 was used to introduce into a UHV chamber for surface analysis a specimen that was electrochemically conditioned in a highly alkaline NaOH solution. Problems with respect to excessive sodium and silica residues were encountered. The NaOH electrolyte was not sufficiently volatile and it extracted excessive quantities of silica from the glass containing components of the apparatus.

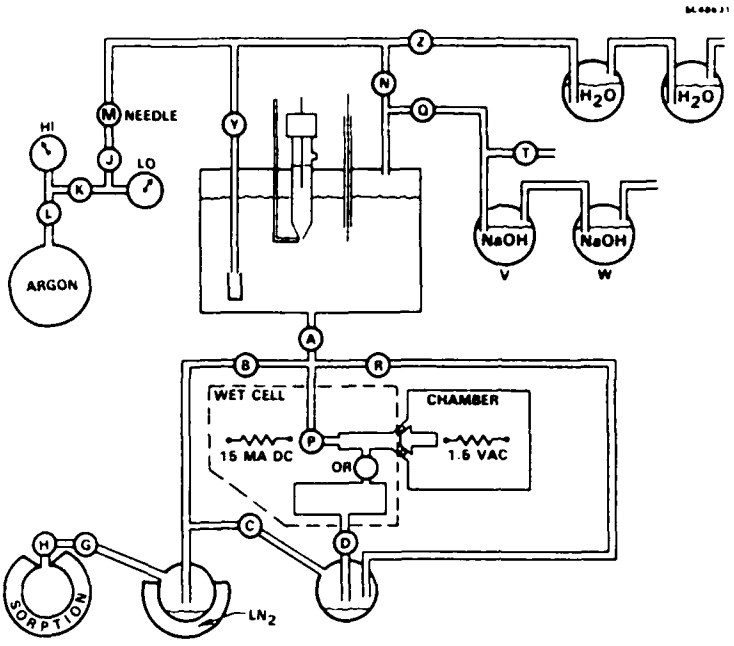

Fig. 5 Schematic for the pre-UHV sample preparation cell.

Recently, some materials changes have been made in the test apparatus and a 0.2% NH_4OH (pH 11.1) was used as the model alkaline medium. This electrolyte provided alkalinity typifying the cathodic crevice beneath a coating, but was sufficiently dilute and volatile to allow it to be easily removed under vacuum. Details of the test procedure appear in Sect. 5.1.

4.3 Wetting

Figure 6a shows the apparatus used to measure the adhesion tension of the liquid of immersion for a cylindrical sample. The adhesion tension, A_{sab}, is defined as F_w/P where F_w and P are defined in Fig. 6b as the wetting force and sample perimeter respectively. In order to examine the role that cathodic reactions have in altering the competition of organic materials with aqueous electrolytes, baseline adhesion tension of the aqueous electrolyte as a function of applied cathodic potential and current has been evaluated for steel. ΔA_{sab} (A_{sab}(open circuit) -A_{sab}(potential)) for a freshly prepared steel surface immersed in air-equilibrated 0.5 M NaCl appears in Fig. 7. As can be seen, ΔA_{sab} increases with applied potential for potentials more negative than

(a)

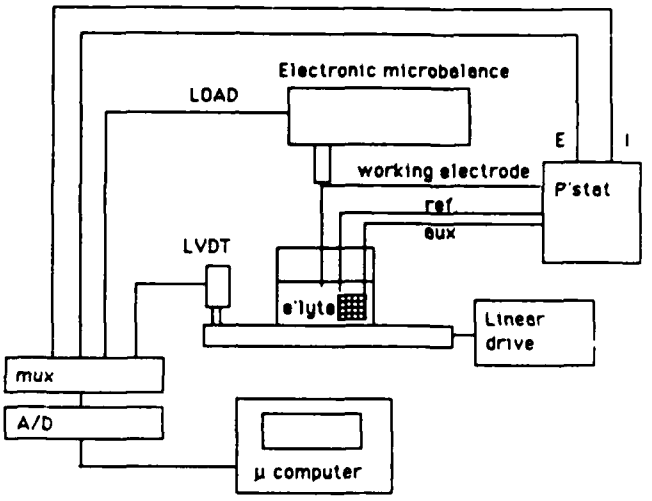

0.4 μm/s to 2 cm/s
displacement resolution < 1 μm
0.1μg resolution (<1 mdyne)

Fig. 6

(a) Surface tension apparatus.
(b) schematic showing the forces on a Wilhelmy plate.

(b)

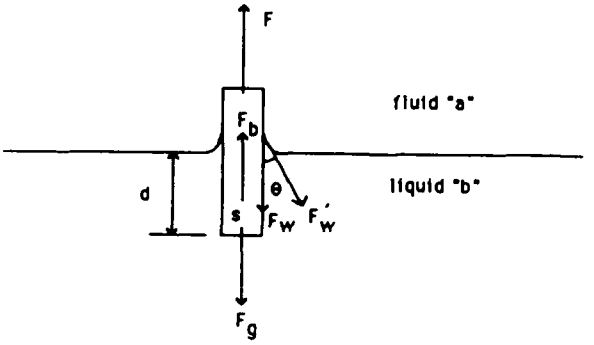

$F = F_g + F_w + F_b$

$F'_w = P\,\gamma_l$ = wetting force of liquid

$F_w = P\,A_{sab} = P\,\gamma_l \cos\theta_{sab}$ = wetting force

$F_g = mg$ = gravitational force

$F_b = -g\pi r^2 d\,\rho$ = buoyancy

P = perimeter of the sample
r= radius of cylindrical sample
d = immersion depth
g = gravitational constant
ρ = liquid density
γ_l = surface tension of the liquid
A_{sab} = adhesion tension

-750 mV vs Ag/AgCl. Hence, the steel appears to become more hydrophilic with increasing cathodic potential. The data for Fig. 7 were obtained after immersing the sample in the 0.5 M NaCl at open circuit. After immersion, the potential was increased at a constant rate and then reversed. As shown in Fig. 7, the increase in ΔA_{sab} is irreversible. Increase in the potential causes an increase in hydrophilic behavior (increased A_{sab}), but reversal of the potential does not return A_{sab} to the initially low and more hydrophobic value.

ΔA_{sab} for steel that was initially passivated at 0 volt vs Ag/AgCl in the pH 9.6 borate buffer and then subjected to a galvanostatic reduction at -220 $\mu A/cm^2$ rapidly increases when the potential reaches -750 mV. At this potential a Fe(III) oxide surface has been converted to a more reduced oxide[19] (Fig. 8). The charge passed to this point is approximately 10 mC/cm^2 which corresponds to roughly 156 A.[19] Assuming a surface roughness factor of 2-2.5, the corresponding oxide film thickness is about 69 A, a reasonable value for an anodically formed film. With conversion to the reduced oxide in the aerated environment, the oxygen reduction reaction then takes over with the formation of sodium hydroxide rather than further reduction of the oxide. The generation of sodium hydroxide most likely catalyzes the wetting process for the rough surface.

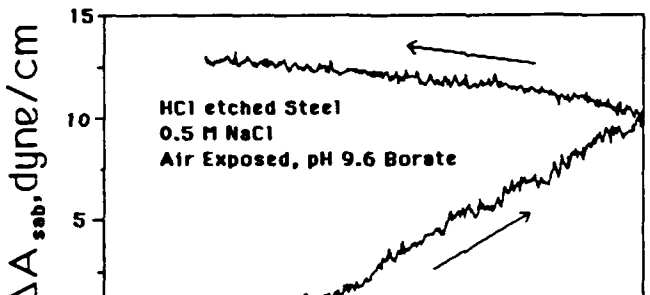

Fig. 7 Change in advancing adhesion tension, ΔA^a_{sab} vs potential for HCl-etched steel in aerated 0.5 M NaCl.

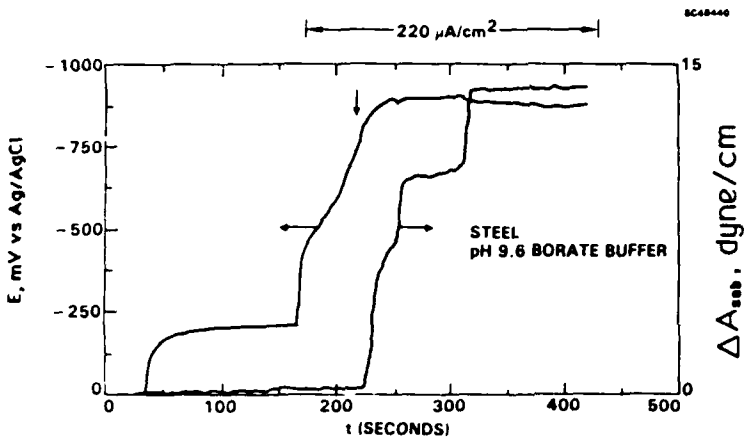

Fig. 8 ΔA^{a}_{sab} and potential vs time during cathodic charging.

5.0 EXPERIMENTAL METHODS

5.1 Pre-UHV Cell for Surface Analysis

Figure 5a shows the cell used to prepare specimens for direct transfer to the UHV chamber for surface analysis. The cell is mounted on a 20 cm stainless steel flange so that it extends into the UHV chamber and is constructed from titanium and PVC. Previously[20,21] glass-filled teflon was used rather than PVC. The use of alkaline solutions which tend to dissolve the silica glass required the change in materials as was determined in the previous year of work. The solution or water rinses can be admitted and expelled from an exterior reservoir system the details of which appear in Fig. 5. There is a small circular opening between the cell and the UHV chamber for inserting the sample. The opening can be vacuum sealed from within the cell by a movable plug and can be sealed from within the UHV chamber with the sample. A saturated calomel reference electrode is used to measure the potential.

By means of a movable plug, the cell is closed to the chamber and is evacuated independently of the UHV system. After achieving UHV, the sample is inserted into the cell opening and gripped in place. Solution is then admitted into the cell from the external reservoir and the plug is retracted to cause immersion of the sample in solution. With valves A and P (the plug) open (Fig. 5b), the sample can be polarized or its potential measured using the cell wall as the counter electrode. When the sample has been exposed to the solution the desired length of time under controlled potential or current conditions, the electrolyte is drained, and rinsed if desired and the remaining liquid is pumped using a sorption pump-trap apparatus; the plug is then inserted from the inside of the cell. The plug and sample surfaces are separated by ~ 0.2 mm when both are inserted. The sample is next removed for analysis. This system allowed Auger electron spectroscopy (AES) and X-ray photoelectron spectroscopy (XPS) of the surface of a carbon steel sample under varied conditions of applied cathodic potential or current in an alkaline 0.2% NH_4OH electrolyte without transporting the specimen through air where the as-prepared reduced state would most likely revert to a more oxidized condition.

5.2 Wetting Experiments

Wetting forces were measured using a Cahn 4000 microbalance and a Rame-Hart variable linear linear drive. For slow extension of specimens into the test liquid, the extension was measured by a LVDT interfaced to a micro-computer which also monitored electrochemical parameters such as potential and current as shown in Fig. 6a. The surface tensions for liquids at various pH were evaluated from the forces on a slowly withdrawn (10 μm/s) freshly flamed and cooled Pt wire. For this measurement the contact angle on the wire at the point of withdrawal from the liquid was assumed to equal zero and hence the observed F_w/P at the point of withdrawal equals the surface tension of the liquid

$$F_w/P = \gamma_l \cos\theta = \gamma_l \qquad (2)$$

The advancing adhesion tension, $A_{sab}{}^a$ (see Appendix) and contact angles for samples having different surface preparations were made from the value of F_w/P after 2 mm immersion of a 0.075 radius steel cylinder test electrode into the test medium. The surface pretreatments appear in Table 2.

Table 2
Surface Treatments

Treatment	Solution	Time/Temp.
Oxalic	40 ml water 20 ml (100g/l) oxalic acid 4 ml 30% H_2O_2	2 × 1 min/50°C
Nitric	Concentrated Nitric Acid	1 min/RT*
HF	Conc. HF (48%)	1 min/RT
Sulfuric	50% of 70% H_2SO_4	1 min
HCl	50% conc. HCl	1 min.

*Following the oxalic acid treatment.

A number of wetting tests were made from a borate buffer test solution containing 0.1 M boric acid and 0.05 M NaOH (pH 9.6). All aqueous solutions were made from reagent grade chemicals and > 16 M Ω cm water processed by a Barnstead Nanopure ion exchange system.

Reagent grade tetra-hydrofuran (THF) and $CHCl_3$ were dried over 5A activate molecular seives. These solvents were used to make solutions of polymethyl methacrylate (PMMA) (Aldrich Chemical Co., Catalog No. 18,225-7, Lot # 03), Polychloride/vinyl chloride copolymer (PVC), (Aldrich Chemical Co., Catalog No. 18,300-8, Lot # AD05), PMMA-Lucite 4F (E.I. DuPont de Nemours). Chemically polished carbon steel cylinders (0.075 mm radius) were exposed to the solutions having varied concentration of the respective polymer. Following exposure the steel cylinder was immersed at a rate of 10 μm/s into pH 9.6 borate buffer to a depth of 2 mm while measuring the force on the cylinder using the Cahn micro-balance.

Reagent grade xylenes were used to make solutions of hydroxy-terminated polybutadiene (Polybd™, Arco Specialty Chemicals, Philadelphia, PA, Lot #604196). The solutions typically contained 0.675% by weight of the polymer. In some cases the Polybd solutions contained 0.6% of a species containing a large organic anion (tall oil fatty acid, Acintol FA2, Arizona Chemical Co, Panama City, FL) or 0.6% of a large organic cation, Adogen 464 (methyl trialkyl(C_8-C_{10}) ammonium chloride, Aldrich Chemical Co., Catalog #85,657-6, Lot #0408PL).

The xylene solutions served as the organic phase in the three-phase wetting experiments whereby the steel cylinder (0.075 mm radius) passed at a rate of 5 μm/s through the organic phase into an aqueous pH 9.6 borate buffer phase under electrochemical control. Continuous measurements of electrochemical potential, current, load, and extension into the liquid for the sample were made using the apparatus in Fig. 6a. The force vs extension data allowed the determination of the adhesion tension, A_{sab}, for the aqueous phase, b, in the presence of the organic phase, a, as defined in Appendix 1. A_{sab} provided a measure of the tendency for the surface-active coating polymer to be displaced by the aqueous phase as a function of applied potential. Control of the potential in the aqueous phase relied on a PAR model 378 potentiostat used in conjunction with a Ag/AgCl reference electrode and a length of Pt wire as the auxiliary electrode. The reference electrode varied by no more than 10 mV against an external standard.

5.3 Electrochemical Impedance

The electrochemical impedance for a carbon steel cylinder (0.075 mm) immersed in the pH 9.6 borate buffer was determined as a function of frequency and potential using the PAR Model 273 Potentiostat and Solartron 1255 Frequency Response Analyzer. The data were collect with the system under control of M388 Electrochemical Impedance Software. The impedance spectra were analyzed using EQUIVCRT Version 3.61.[22] The frequency dependent complex impedance Z(s) was fit by adjusting the parameters Y_o, n, R_1 , and R_2:

$$Z(s) = R_1 + R_2/(1 + R_2 Y_o s^n) \quad (3)$$

where $s = j\omega$, $j^2 = -1$. ω is the angular frequency in radians/s. R_1 equals the solution resistance and R_2 represents the polarization resistance. Y_o is a constant related to the capacitance, Cd, by:

$$C_d = Y_o^{1/n} R_2^{(1-n)/n} \quad (4)$$

assuming that the characteristic time for the electrochemical relaxation equals R_2C_d.[22] Electrochemical impedance measurements were made under potentiostatic control using a ± 10 mV modulation. Five data points were collected/decade of frequency change from 10 kHz to 10 mHz for oxalic acid polished steel in pH 9.6 borate buffer.

6.0 DETAILS OF RECENT RESULTS

6.1 Results for Wetting Experiments

Figure 9 shows a plot of surface tension vs pH for water adjusted to different pH with the addition of NaOH. Since the solutions were not buffered a drift in pH for the cases near neutral were observed. This variation in pH was monitored by a pH measurement made before and after the wetting experiment. The surface tension was taken as the maximum receding force divided by the sample perimeter and corrected for gravity and buoyancy on a pre-flamed Pt wire as it is withdrawn from the solution. This force equals the surface tension of the liquid assuming the contact angle of the liquid on the specimen is zero. This is a very good assumption for a well cleaned Pt wire as it recedes from an aqueous solution. As can be seen from the plot in Fig. 9, the surface tension of water decreases as the pH increases above neutral. The lowering of the surface energy of the liquid as a result of a surface excess of the electrolyte will enhance its ability to wet the steel surface. Thermodynamic considerations (Gibbs) dictate that a surface excess of the solute (NaOH) exists. Alkalir conditions, therefore, favor the presence of NaOH at the surface of the electrolyte and wetting of the surface.

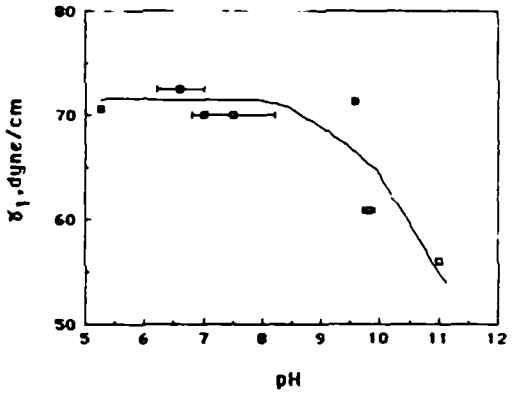

Fig. 9

Surface tension of water as a function of pH.

The role of surface roughness in wetting has been a subject of conflicting reports, most likely as a result of the large hysteresis in wetting of rough surfaces. Advancing contact angles on rough surfaces are, in general, much lower than receding contact angles. Wenzel[24] reports that the contact angle of wetting liquids will decrease for rough surfaces, while more recent work[25,26] reports that surface roughness increases

advancing contact angles due to the need to overcome the energy barriers produced by asperities (demanding low microscopic contact angles for the liquid to advance). This appears to be the case for steel in contact with the pH 9.6 borate solution as shown by the data in Table 3 and Fig. 10. The steel was prepared by the treatments of Table 2. Carbon steel plate with the treatments of Table 2 give surface profiles shown in Figs. 10. As can be seen the surface roughness on the 100 μm scale is considerably less for the nitric acid and oxalic acid treatments giving advancing contact angles of 0 and 34°, respectively, while the rougher HCl and sulfuric acid etched surfaces give high advancing contact angles of 76 and 120°. This correlates with the rms roughness data, R_a, as measured on actual test cylinders (Table 3). The R_a values represent the average obtained from at least five 300 μm scans of the test cylinders using a Dektak 3030 Profilometer. The plus or minus deviations are the calculated standard deviation of the respective averages. As can be seen the rougher surfaces tend to be more hydrophobic giving higher advancing contact angles θ. All samples were treated in the respective solution after first chemically polishing in the oxalic acid solution (Table 2). It was found that the nitric acid treatment (a passivation) produced no additional roughening by itself and, therefore, its roughness depended entirely on the preceding oxalic acid etch. The HCl and sulfuric acid treatments roughened the surface.

Table 3

Adhesion Tension and Calculated Contact Angle for Advancing pH 9.6 Borate on Steel Surfaces

Treatment	A^a_{sab}, dyne/cm	θ, degrees*	R_a, μm
Oxalic	66	0	0.16 ± 0.06
Sulfuric	-33	120	0.56 ± 0.1
HCl	16	76	0.24 ± 0.04
Nitric	55	34	0.13 ± 0.03

*Assuming δ for liquid of 66 dyne/cm (Fig. 9).

It is most likely that the effect of applied potential on the wetting of steel (Fig. 7) can be explained by localized lowering of the surface tension of the liquid due to the generation of base at the surface (see Fig. 9) thereby enabling the meniscus to overcome the asperities. Hence, cathodic polarization will catalyze the advancing of the

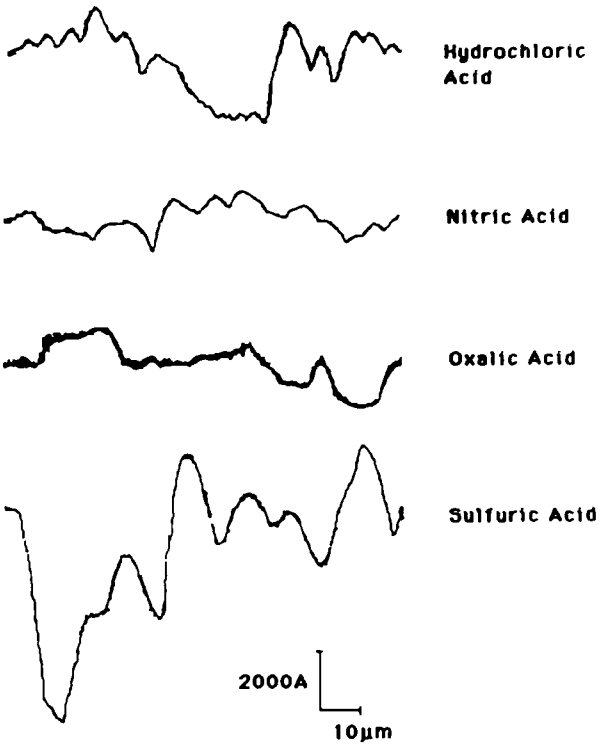

Fig. 10

Surface profiles for chemically treated steel surfaces for 100 μm scans.

menicus, but reversal of the potential will not reverse the observed surface force as shown in Fig. 7. Teschke and coworkers[27] recently invoked a change in surface concentration brought about by high anodic dissolution of iron and Al in 1 M H_2SO_4 for increasing a wetting force (A_{sab}). While the system under consideration here differs from the rapidly dissolving metals in concentrated acid, the principle of a local build-up in the concentration of a surface species which lowers surface tension of the liquid and hence alters A_{sab} applies for both cases.

The results for the potential influenced wetting of steel by aqueous electrolytes demonstrate an important factor in the mechanism of cathodic disbonding, the fact that cathodic generation of base sufficiently lowers the surface tension of the liquid so as to enhance the rate of wetting of the steel by the electrolyte. Questions remain as to whether and by what mechanism cathodic polarization displaces the organic films and polymers from the steel surface. To address these question, a series of experiments were performed to establish: (1) the mechanism of the displacement of an inert organic layer from steel in the presence of electrolyte as a function of applied potential, and (2) the role of specific polymer/metal interactions in this process.

Figure 11 shows the force/perimeter ratio, F/P, for an oxalic acid chemically polished steel cylinder immersed and extracted at 5 μm/s from a fluid comprised of approximate 0.15 cm layer of xylene over a pH 9.6 borate electrolyte. As the sample passes into the xylene layer (0.03 cm in Fig. 11), a force corresponding to 28 dyne/cm appears on the metal directed into the liquid. This force divided by the perimeter equals the surface tension of the liquid indicating a zero degree contact angle for the xylene on the steel. As the sample passes through the xylene phase a linear decrease in F/p with extension results due to the linear increase in buoyancy with depth. Upon passing into the borate phase (at about 0.2 cm in Fig. 11) a time-varying force in excess of the buoyancy tending to expel the specimen is felt by the sample as evidenced by a decrease in the force at a rate greater than the decrease due to increased buoyancy. This hydrophobic force comes to equilibrium with a return to the linear decrease in force with extension due to buoyancy at an immersion of about 0.4 cm (Fig. 11). The equilibrium F/p corrected for buoyancy gives the adhesion tension of the electrolyte for the steel in the presence of the xylene phase under advancing conditions, A^a_{sab}, as illustrated in Fig. 11. Upon the start of withdrawal of the specimen, a rise in F/p occurs. F/p for the receding miniscus then comes to steady state exhibiting the linear change due to diminishing buoyancy as the sample is withdrawn (Fig. 11). As the sample passes into the organic xylene layer it pulls up the borate meniscus. The difference between the steady state F/p for the receding sample corrected for buoyancy, and the F/p for the specimen in the xylene layer as corrected for buoyancy gives the adhesion tension of the electrolyte for steel in the presence of the xylene under receding conditions, A^r_{sab}, as illustrated in Fig. 11.

For Fig. 11 no potential was applied to the specimen as it passed into the aqueous layer. The open circuit potential for the specimen as it passed into the aerated, pH 9.6, 0.1 M boric acid/0.05 M NaOH achieved a steady value of -260 mV vs Ag/AgCl. For an applied potential of -1100 mV vs Ag/AgCl, the results (Fig. 12) differ considerably from the open circuit case of Fig. 11. In the first instance, upon moving into the aqueous phase, F/p immediately increases. However, there is a large amount of fluctuation as the sample moves into the aqueous phase. The xylene meniscus seems to stick and then recede. When the meniscus of the xylene layer sticks, F/p decreases. F/p rises rapidly as the xylene layer recommences recession with advancement of the sample through the interface.

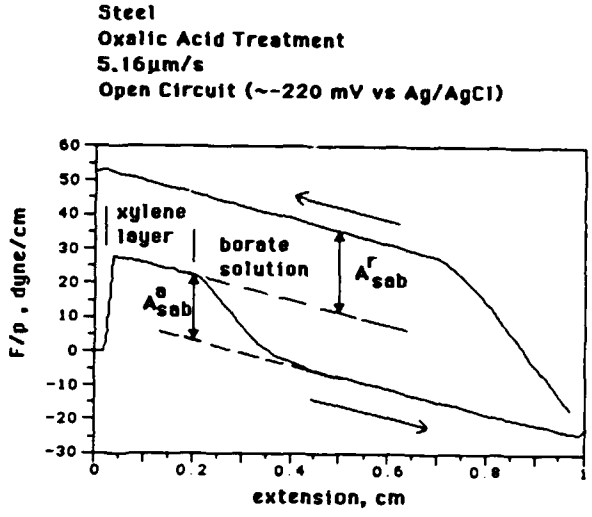

Fig. 11

F/p vs Extension for the chemically polished (Oxalic acid/peroxide) steel passing through the interfaces formed by air/xylene/borate. The steel is at open circuit in the borate phase.

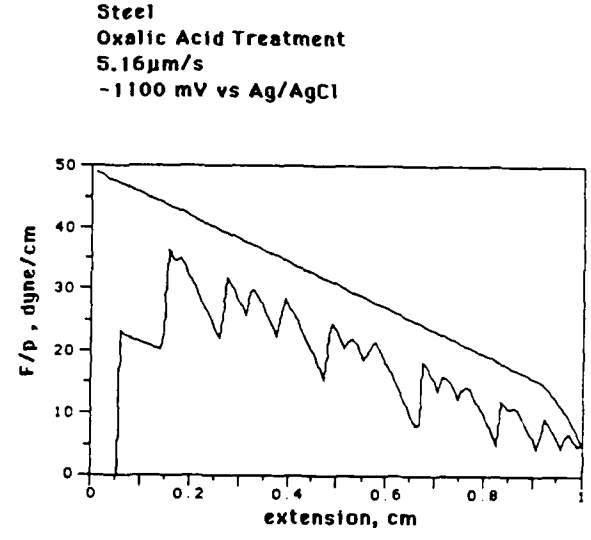

Fig. 12

F/p vs extension for the chemically polished (Oxalic acid/peroxide) steel passing through the interfaces formed by air/xylene/borate. The steel is polarized at -1100 mV vs Ag/AgCl in the borate phase.

Subtracting the linear component of F/p (correcting for buoyancy) and subtracting a linear component of the observed current (effectively normalizing for area exposed to the aqueous phase) results in the time dependent fluctuations δA^a_{sxb} and δI in adhesion tension and current respectively (Fig. 13). Note that a cathodic current spike occurs coincident with each increase in δA^a_{sab}. The increase in current occurs as the organic meniscus pulls back exposing fresh surface. The current spike may be a combination of faradaic and non-faradaic current (charging of the double layer).

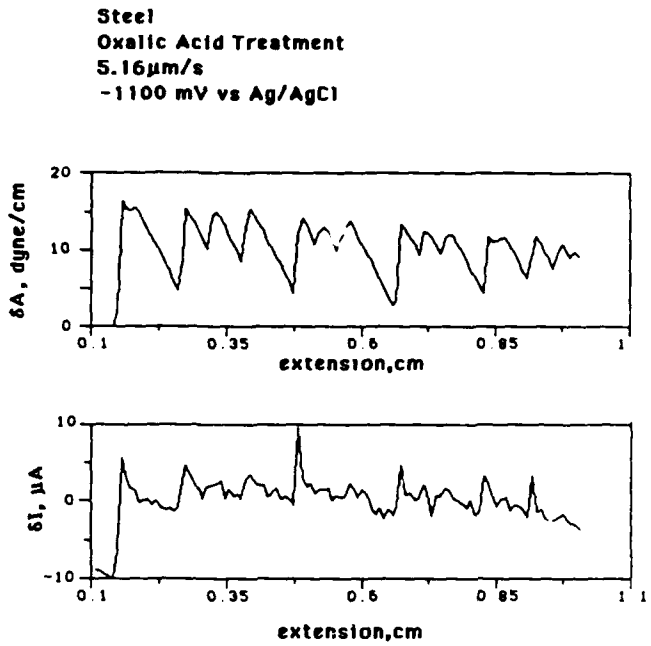

Fig. 13

Current fluctuations and adhesion tension fluctuations for the experiment of Fig. 12.

Figure 14 summarizes the observed potential dependence for the advancing (a) and receding (b) adhesion tension for the electrolyte contacting the steel in the presence of xylene. For the advancing contact, the adhesion tension for the aqueous phase decreases to values below zero (hydrophobic interaction) for sufficiently high potentials (above -600 mV vs Ag/AgCl), but increases to relatively high values of 30 dyne/cm at -1000 mV (hydrophilic). The receding adhesion tension remains relatively high, but a minimum appears between -600 and -800 mV. The steel becomes slightly more susceptible to wetting by the aqueous phase (higher A) under both cathodic and anodic polarization away from the -600 mV minimum. However, A^r_{sab} decreases again at -350 mV.

The second phase of the wetting work focused on the displacement of an organic polymer by an alkaline electrolyte. These experiments were designed to pinpoint the molecular process involved in coating deadhesion. Initially experiments focused on the role of surface acid/base behavior. A typical acidic polymer (PVC) and a basic polymer (PMMA) were used as surface probes. These polymers could not be dissolved in neutral CCl_4 following the approach of F. Fowkes.[28] The acidic polymer could easily be dissolved in a basic solvent (THF) and the basic polymer was dissolved in an acidic solvent ($CHCl_3$). However, the basic polymer could also be dissolved in THF. Freshly chemically polished (Oxalic acid treatment in Table 2) and dried steel samples were

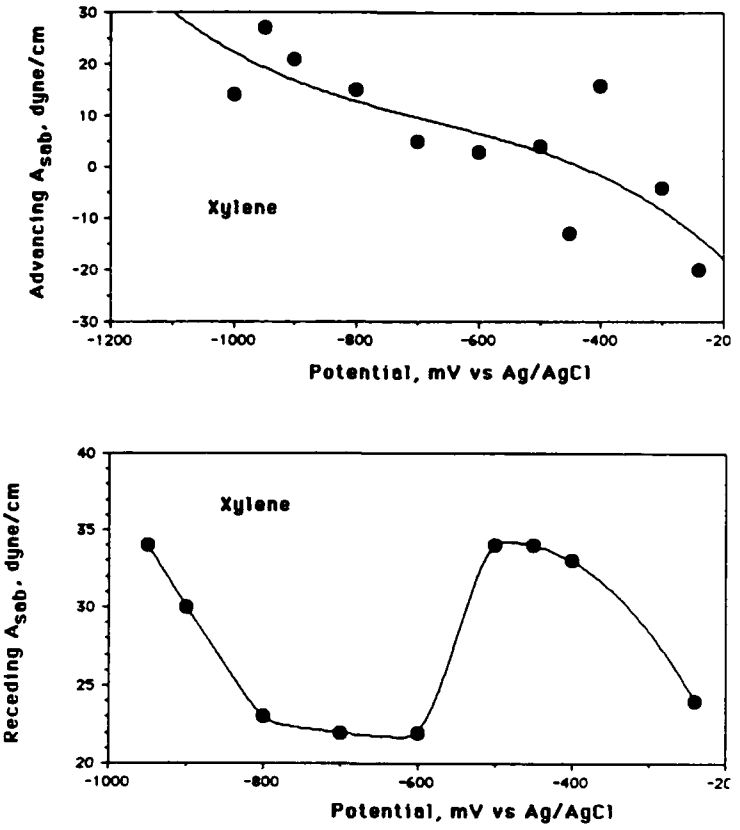

Fig. 14

Advancing and receding values of A_{sab}. Fluid "a" is xylene, fluid "b" is 0.1 M aerated boric acid/ 0.05 M NaOH in water. The sclid "s" is a 1010 steel cylinder chemically polished in the oxalic acid/peroxide at 50°C.

equilibrated for several hours in solutions having weight fractions varying from 10^{-10} to 0.1. The samples were removed from the polymer solution and blow dried followed by a measurement of the advancing adhesion tension from force vs extension curves as the sample passed at open circuit into the borate solution to a depth of 0.2 cm. For very dilute polymer solutions little polymer adsorbed onto the steel surface. As a consequence, the adhesion tension for the electrolyte/steel interface was high, approaching the maximum 66 dyne/cm (surface tension for the pH 9.6 the borate electrolyte) (Fig. 15). The metal remained hydrophilic. For both the PMMA in THF and the PVC in THF, the observed adhesion tension for the electrolyte decreased when the steel was treated in polymer solutions above a weight fraction of $3 \cdot 10^{-4}$. The transition of the metal from hydrophilic to hydrophobic occurred at the $3 \cdot 10^{-4}$ weight fraction for both polymers in THF (Fig. 15) showing that the free energies for the adsorption of the

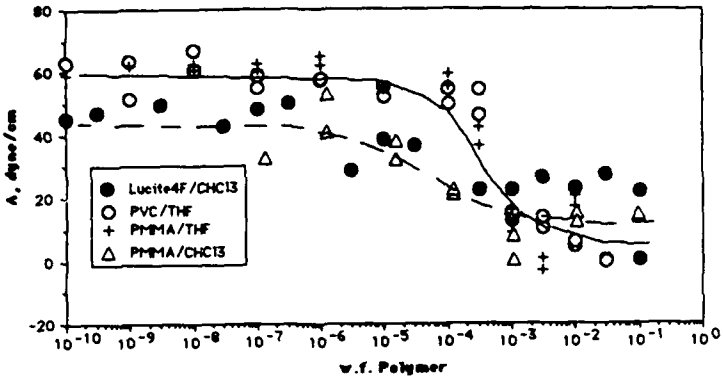

Fig. 15 Advancing adhesion tension of the electrolyte for steel (air/steel/borate) vs polymer concentration of a pre-treatment solution.

polymers on the steel surface from the basic THF were identical*. No particular preference of the steel to absorb the acidic polymer from the basic THF solvent, or the basic polymer (PMMA) from the basic THF was observed. The basic THF excluded both of the polymers from the steel surface to an equal extent. On the other hand, PMMA in the acidic $CHCl_3$ solvent shows a somewhat greater tendency to absorb onto the steel surface. Note that the transition from wetting to non-wetting for PMMA in $CHCl_3$ occurs at $2 \cdot 10^{-5}$ w.f. for the polymer** in the $CHCl_3$ as compared $3 \cdot 10^{-4}$ w.f. of the PMMA in the basic THF. This corresponds to a more favorable energy of adsorption of the PMMA from the $CHCl_3$ by about 5.7 kJ/mol* as compared to absorption from THF. The surface competes more successfully with the acidic $CHCl_3$ solvent for the PMMA as compared to competition by the surface with the basic THF for PMMA. The steel surface appears, therefore, to be weakly acidic by the arguments of Fowkes.[28] This is consistent with the chemically polished (oxalic acid) surface containing more of an acidic iron(III) oxide as opposed to the more basic iron(II) oxide.[29] XPS analysis for the Oxalic acid treated surface confirms that the surface contains some Fe(III) oxide species (Sect. 6.2). More data along these lines are needed to completely characterize the acid-

*The free energy of adsorption will be proportional to the log of a concentration for 1/2 a monolayer of adsorbate, a_c according to the equation: $dG = 2.303RT \log a_c$. For the experiments performed with the polymer solutions the concentration for the transition from hydrophobic to hydrophilic is taken as a_c.

**Both the Aldrich PMMA and the Lucite 4F, a commercial PMMA resin.

base properties of the test surface. Nevertheless, it seems reasonable to hypothesize that the best polymer metal interaction for the oxalic acid treated surface occurs when the polymer is slightly basic.

While the experiments of Fig. 15 provide information on the basic interaction of the polymer with the slightly acidic steel surface, a more detailed understanding of the processes that take place during the displacement of polymers from metallic surfaces under electrochemical polarization is required for analysis of the mechanism of cathodic disbonding. Hence, wetting experiments similar to those of Fig. 11 were performed, but with the organic xylene phase containing a model polymer solute (Polybd).

Figures 16a-g show the resulting F/p vs extension curves for a set of experiments with the xylene layer containing 0.675 weight % of the hydroxy-terminated polybutadiene (Polybd). As can be seen in Fig. 16, two distinct curves result. Curves for potentials positive to -600 mV (Fig. 16 a-b) exhibit little hysteresis and the sample remains hydrophobic (a decrease in F/p in the electrolyte phase) even upon its withdrawal. However, considerable hysteresis occurs in the force vs extension curves for potentials of -600 mV (Fig. 16c) and more negative (Fig. 16d-g). While the advancing behavior (taken during sample immersion) mimics that for the samples above -600 mV, the sample becomes rather hydrophilic upon withdrawal for potentials of -600 mV and below.

The results for the wetting experiments of Fig. 16 are summarized in Fig. 17 in terms of the potential dependence of A^a_{sab} and A^r_{sab}, the advancing and receding adhesion tensions for the electrolyte to the steel in the presence of the polymer-containing organic (xylene) layer. A^a_{sab} remains negative and nearly potential independent showing uniform hydrophobic behavior for the steel as a result of polymer adsorption at the surface. However, with receding contact, A^r_{sab} is near zero dyne/cm for potentials above -600 mV while below -600 mV, A^r_{sab} steps to about 10 dyne/cm. These results show that the hydrophobic behavior is retained even after passing through the electrolyte when the potential is sufficiently high, but cathodic polarization to potentials more negative than -550 mV causes the sample to become hydrophilic evidenced by an increased A^r_{sab}. The transition from hydrophilic to hydrophobic occurs sharply at -550 mV vs Ag/AgCl. Above -550 mV the polymer remains irreversibly adsorbed on the steel, keeping it hydrophobic, whereas below -550 mV the polymer desorbs and the steel becomes hydrophilic for receding contact.

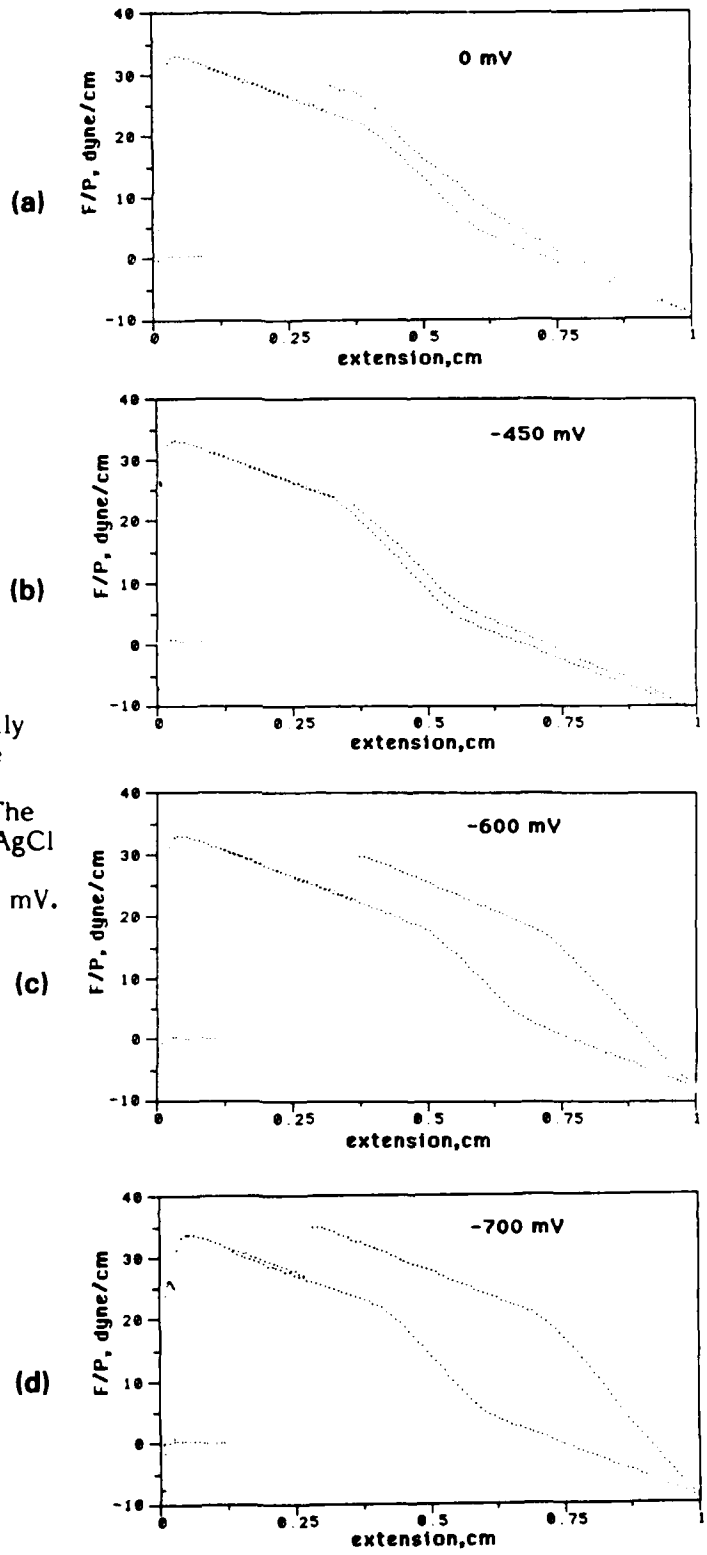

Fig. 16

F/p vs extension for the chemically polished steel passing through the interfaces formed by air/xylene (0.675% Polybd)/pH 9.6 borate. The steel is polarized relative to Ag/AgCl in the borate phase to (a) 0 mV, (b) -450 mV, (c) -600 mV, (d) -700 mV.

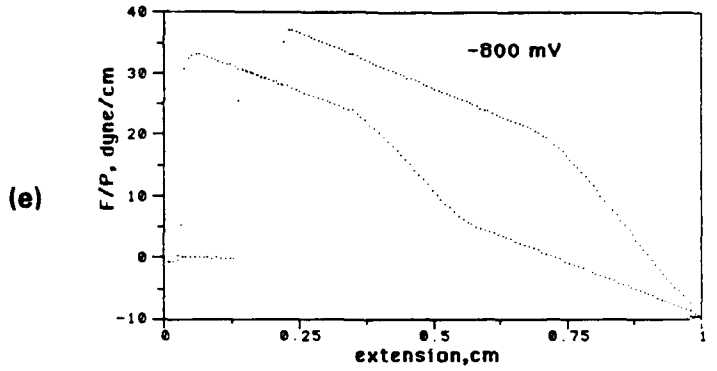

(e)

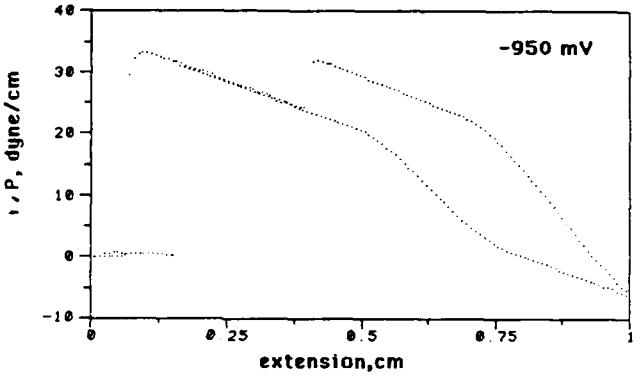

(f)

Fig. 16 (continued)

(e) -800 mV, (f) -950 mV, (g) -1100 mV.

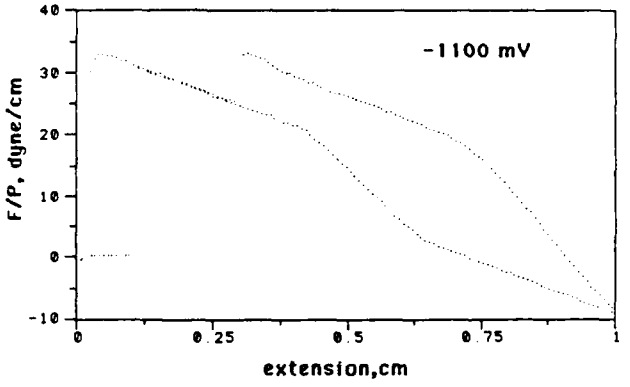

(g)

The integrated Faradaic charge, Q, that passes during the wetting experiment as a function of potential appears in Fig. 18 along with A^{r}_{sab}. Q measures the extent of the cathodic reaction during the test. For potentials more negative than -1000 mV the charge rapidly increases as the hydrogen formation starts to dominate the electrode kinetics. Below this potential the predominant reaction is the oxygen-limited

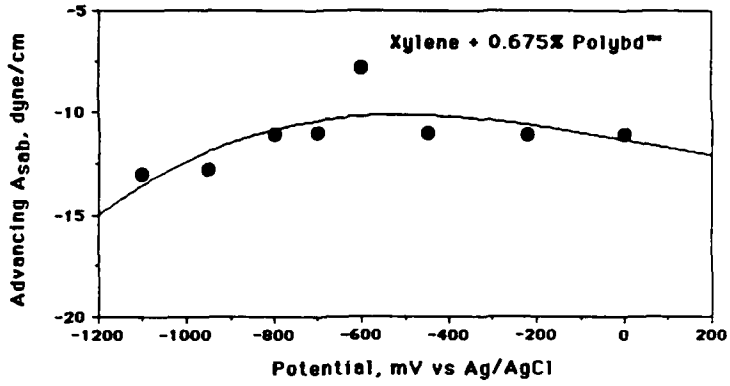

Fig. 17

Advancing and receding values for A_{sab} for the steel/xylene phase/borate interface as a function of potential of the steel in the borate phase.

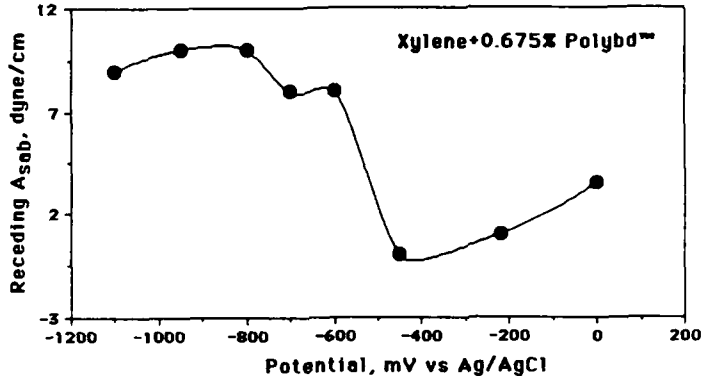

Steel - oxalic/peroxide chemical polish
0.1 M boric acid/.05 M NaOH
Air exposed

Fig. 18

Total Faradaic charge/cm², Q, and A^r_{sab} vs potential for the experiments of Fig. 16.

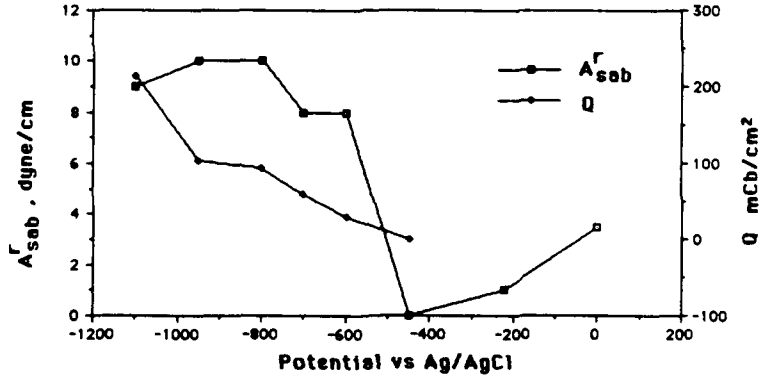

reduction. A^r_{sab} shows a step between -450 and -600 mV and does not increase for more negative potentials. A^r_{sab}, therefore, does not appear to directly follow the cathodic reaction.

The sharp change in the wetting behavior as measured by A^r_{sab} over a very short potential region around -550 mV vs Ag/AgCl suggests that the ability of the electrolyte phase to displace the polymer as adsorbed from the xylene solution relates to the potential of zero charge (pzc) for the steel. Below the pzc the steel attains a negative charge and tends to displace a polymer that has a negative zeta potential, whereas above the pzc the positively charged steel surface retains a good bond to the adsorbed polymer.

The Lippmann-Helmholz equation relates the surface tension for the solid surface to the double integral of the double layer capacitance, C_d:

$$\gamma_s = -\int[\int C_d \cdot dE]dE \qquad (5)$$

and the excess surface charge as the integral of the double layer capacitance:

$$Q_s = -\int C_d \cdot dE \qquad (6)$$

The constants of integration will depend on the potential of zero charge, pzc. Figure 19 shows the observed double layer capacitance for the steel in the test electrolyte as a function of potential. Performing the integrations with the assumption that the pzc equals -550 mV as suggested by the location of the step in the A^r_{sab} vs potential curve (Fig. 17) provides the constants of integration and allows determination of the potential dependences for the surface charge density, Q_s (Fig. 20), and the metal surface tension γ_s (Fig. 21). As can be seen by this analysis, the surface tension for the steel decreases quite dramatically upon cathodic polarization where a negative surface charge is present. Under cathodic polarization the work required to form a metal surface, $\gamma_s \cdot dA$ is substantially less than that for the more anodic potentials. This may contribute to the tendency for adhesive failure of organic coatings on steel.

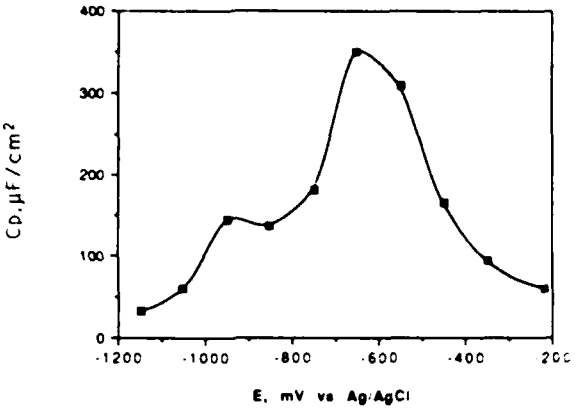

Fig. 19

C_d vs potential for steel in 0.1 M pH9.6 borate.

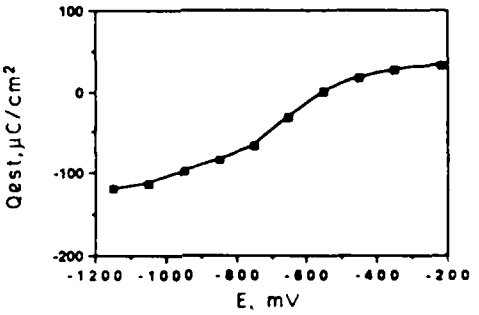

Fig. 20

Estimated surface charge Q_s from the integration vs potential for steel in 0.1 M pH9.6 borate.

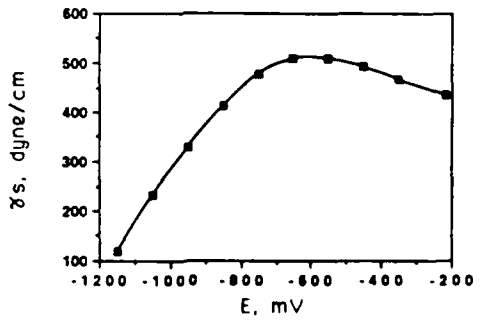

Fig. 21

Calculated γ_s for steel in borate as a function of potential.

The preceding analysis also shows that at cathodic potentials more negative than -550 mV vs Ag/AgCl in pH 9.6 borate the steel surface has a net negative charge that repels the polymer. The polymer must, therefore, have a negative zeta potential. Small quantities of fixed residual negative charge within the polymer most likely contribute to the negative zeta potential.

The question can be asked: can the adhesion of the organic film to the steel be improved with the presence of fixed positive charge in the polymer film? Accordingly, a large molecular weight organic cation, the long chain alkyl quaternary ammonium compound, Adogen™ 464, was dissolved in the organic phase along with the Polybd polymer. F/p vs extension for the steel sample as it passes through the respective liquid layers with a polarization to -1100 mV in the electrolyte layer appears in Fig. 22. The Adogen™ decreases the surface tension of the xylene/electrolyte interface, γ_{xe}, as compared to that for the xylene solution of the polymer containing no Adogen™. As a result no dramatic decrease in F/p occurs when the sample traverses the organic/aqueous interface as occurs for the solution with no Adogen™ (compare Fig. 22 with that for Fig. 16g). However, as the sample is withdrawn from the solution, F/p increases only at a rate consistent with buoyancy changes (Fig. 22). No dramatic increase in F/p at reversal occurs. This differs from the observation for no Adogen™ (Fig. 16g) where a large increase in F/p occurs. For the sample with no Adogen™, the receding adhesion tension for the aqueous phase with the metal in the presence of the organic layer (A^r_{sab}) is about 10 dyne/cm, but there is no measurable adhesion tension of the electrolyte for the sample surface when the organic phase contains the positively-charged large organic cation (Adogen™ 464) (compare Figs. 16g and 22, respectively).

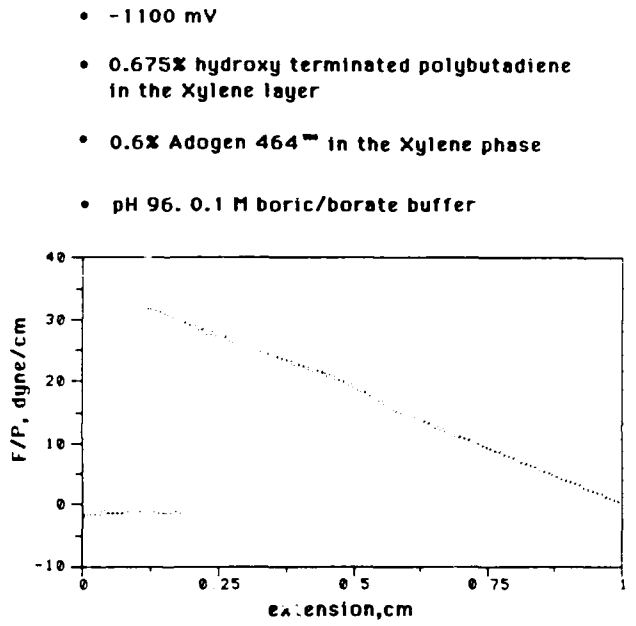

Fig. 22

F/p vs extension for the chemically polished steel polarized at -1100 mV vs Ag/AgCl and passing through the interfaces formed by air/xylene (0.675% Polybd+0.6% Adogen 464)/ borate.

This result has important implications for designing polymer coatings for optimum cathodic disbonding resistance. Clearly an organic coating, that has a positive zeta potential, produced, for example, by a small concentration of positive fixed charges grafted onto the polymer backbone, would be expected to have enhanced adhesion to the steel under cathodic conditions. Several caveats to this statement must be made, however. First, positively fixed charge must have a a benign anion. While OH^-, borate, phosphate or a number of inhibitor anions such as chromate and molybdate may be beneficial, there is always the possibility that such sites can serve as exchange sites for chloride ion which usually has a detrimental effect***. In the second place, an organic coating with negatively fixed charge may loose adhesion under anodic conditions and would certainly be a less basic and most likely acidic polymer. Note, however, that cathodically deposited organic coatings have superior corrosion resistance as compared to anodically deposited organic coatings.[30] This fact supports the arguments made above that better adhesion will result from the presence of residual positive charge at the coating metal interface. Development of polymer coatings with a small concentration of fixed positive charge might be accomplished by grafting quaternary ammonium functionality onto the polymer backbone.

6.2 Results for the Surface Analysis

Knowledge of the surface chemistry of carbon steel under cathodic disbond conditions will lend important support or provide critical data to the proposed mechanism of cathodic disbonding. In order to establish the surface chemistry of carbon steel in an environment simulating the cathodic disbond zone, steel samples were treated electrochemically in the cell described in Fig. 5 and Section 5.1. The particular objective of this phase of the program has been to determine the chemistry of the iron compounds that are stable on the carbon steel surface under cathodic disbond conditions.

The electrolyte used was 0.2% NH_4OH (pH 11.1). This dilute electrolyte was chosen to provide an alkaline environment while being sufficiently dilute to play a

***Note that Agarwala[38] used Adogen™ with borate, molybdate, dichromate and nitrite as a water displacing corosion inhibiting system. His approach provides some of the motivation for the approach described here. The ability of the compound to render cathodic sites hydrophobic might explain its ability to inhibit the hydrogen caused SCC of high strength steel.

minimal adsorption role. Most importantly, the electrolyte was entirely volatile and was readily removed in the vacuum. Auger electron spectroscopy (AES) detected virtually no nitrogen on the test surfaces. Previous work using a concentrated NaOH electrolyte resulted in steel surfaces heavily contaminated with residual Na_2O and silicon compounds. The silicon compounds were leachates from the glass of the test cell. A redesign of the test cell eliminated much of the pyrex glass previously used. However, not all of the glass could be eliminated since some parts of the cell had to be transparent so that the operator could gauge the presence of electrolytes and gas bubbles.

Figure 23 shows the iR drop corrected current vs potential behavior of the steel in the electrolyte. There was a considerable iR drop in the test cell (a solution resistance on the order of 2000 Ω was observed by interruption methods). However polarization potentials were corrected using externally determined current density vs potential data. A current vs potential curve obtained using a PAR cell with a Luggin capillary located close to the specimen sufficiently minimized ohmic drop so as to provide a relationship between current density and potential. This data was used to determine the potential attained in the pre-UHV cell from the current density of the sample. As seen in Fig. 23 a current below 10 $\mu A/cm^2$ flows until the sample reaches a potential of -1000 mV vs SCE (-955 mV vs Ag/AgCl) at which point water reduction to hydrogen dominates the reaction.

Fig. 23

Potential vs log current density for steel in deaerated 0.2% NH_4OH (IR-drop corrected).

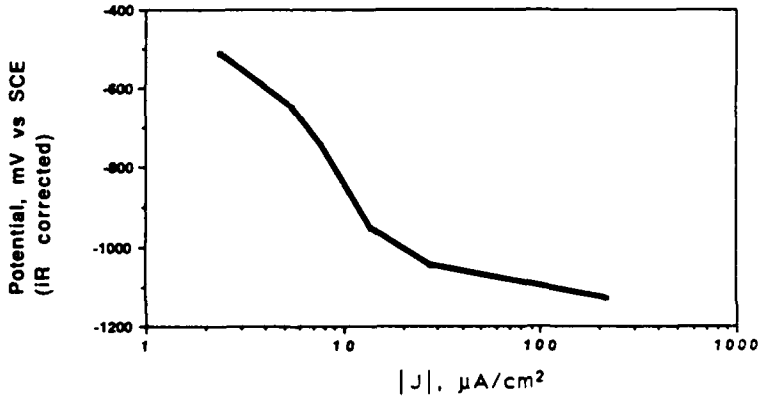

The sample was Ar-ion etched and then transferred to the conditioning cell where it was immediately polarized to the test potential. The polarization continued for 10-15 min until constant currents were observed. The electrolyte was then removed and the sample placed directly in the UHV as described in Sect. 5.1. Auger electron spectra (AES) were immediately taken to characterize the overall chemistry of the surface. It was found that Si remained as a major component on the surface which showed a possible tendency to concentrate under conditions of higher cathodic polarization (Fig. 24). Clearly the elimination of the Si contamination was not achieved.

Fig. 24

Atom ratio of Si to Fe vs potential of the pretreatment.

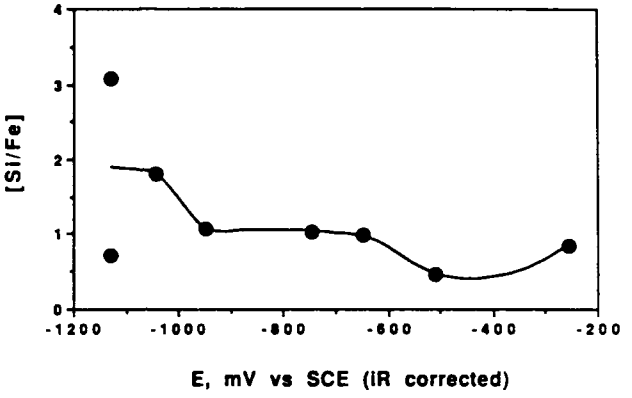

Despite the Si contamination the iron chemistry could be characterized from the Fe 2p XPS spectra for different pretreatment potentials shown in Fig. 25. Several features are apparent from the spectra. For the sample at open circuit (-256 mV), the spectrum is primarily that for Fe_3O_4 as determined from the energies of the two Fe 2p peaks. However, there is a slight increase in intensity between 714 and 719 eV which indicates the presence of FeOOH. This type of spectrum was also observed for the sample chemically polished in Oxalic acid/peroxide (Fig. 25b). In addition intensity from the Fe(0) substrate as evidenced by the low energy shoulders at 707 ev and 721 eV shows that the oxide on the sample prepared at open circuit in the pre-UHV cell is extremely thin.

At -400 mV, the intensity between 714 eV and 719 eV due to Fe(III) has vanished entirely, but the Fe(0) soulders remain. This spectrum remains essentially the same until -1130 mV where currents on the order of -100 $\mu A/cm^2$ were observed. At this

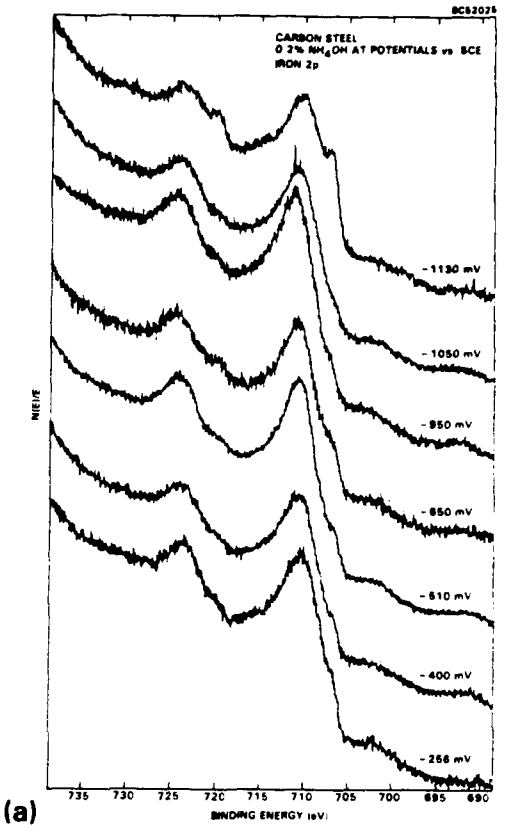

Fig. 25

(a) Iron 2p XPS spectra for carbon steel as a function of the preparation potential; (b) Iron 2p XPS spectrum for Oxalic acid/peroxide treated steel.

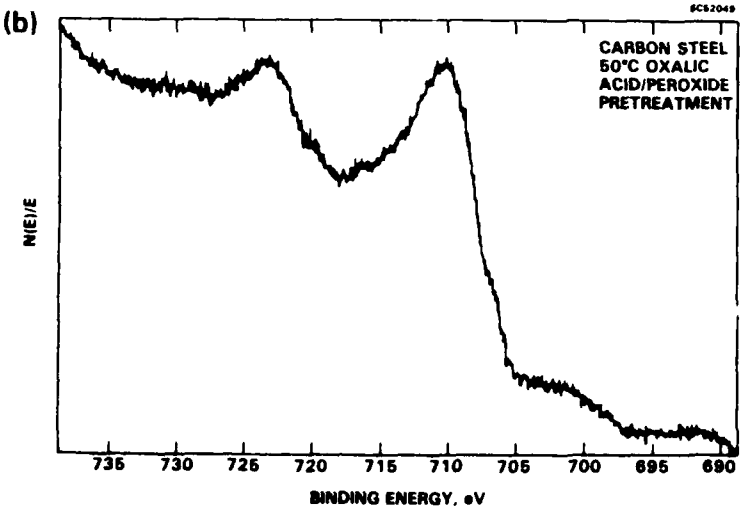

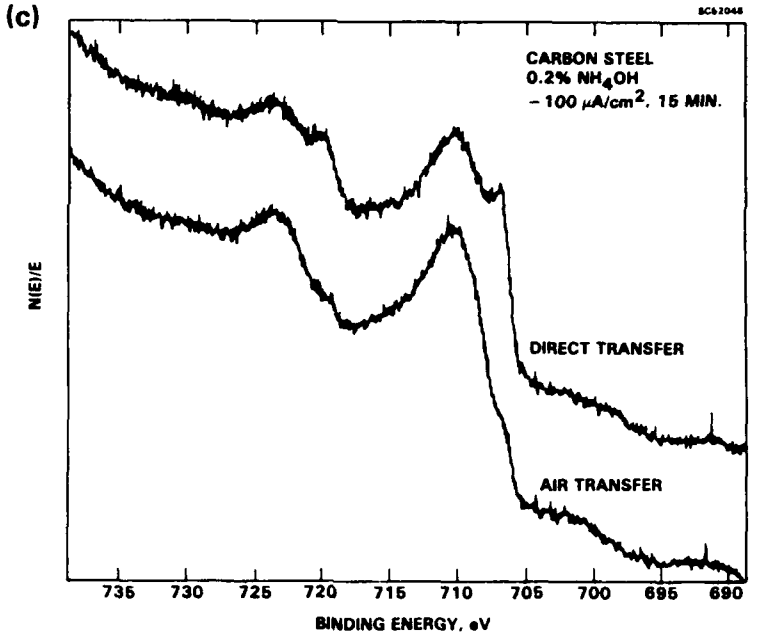

Fig. 25 (continued)

(c) Iron 2p spectra for carbon steel treated at $-100\ \mu A/cm^2$ before transfer to the UHV. The air transfer was made through laboratory air while the direct transfer relied on the pre-UHV cell.

point the oxide is reduced to produce distinguishable low energy $2p^{1/2}$ and $2p^{3/2}$ peaks for the metal in the zero oxidation state. Between -250 mV and -650 mV(SCE) of sample pre-treatment, the Fe $2p^{3/2}$ line is in the 710.6 to 711 eV region which is relatively high and suggests that the Fe_3O_4 is slightly oxidized.[31] At -950 mV of pretreatment in the alkaline electrolyte, the Fe $2p^{3/2}$ shifts to lower energies by a few tenths of an eV while at -1130 mV ($-100\ \mu A/cm^2$) distinct peaks for the metallic state appear. An identical treatment (at $-100\ \mu A/cm^2$) followed by air transfer gave a spectrum shown in Fig. 25c as compared to the direct transferred sample from the pre-UHV cell. As can be seen no Fe(O) peaks are present for the air transferred specimen which illustrates the utility of the pre-UHV cell for preserving the surface chemistry.

To summarize, the iron XPS results show that an extremely broad cathodic region exists between -400 and -1100 mV where Fe_3O_4 is stable. Positive to -950 mV the oxide is slightly oxidized. Distinct Fe(III) oxides, however, do not appear in the surface and the Fe(0) component is considered to be under the film in the -400 to -1100 mV(SCE) region. The oxide reduces for potentials more negative than -1100 mV and the Fe(III) appears at potentials more positive than -260 mV vs Ag/AgCl. This broad region of stability for a nominal Fe_3O_4 calls into question the oxide reduction mechanism as being of great significance in freely corroding steel for causing cathodic disbonding. Certainly

the oxide reduces at high cathodic current densities (>100 $\mu A/cm^2$). However, these conditions are not present in the -800 to -950 mV (SCE) region where severe cathodic disbonding commences (ca. -750 to -900 mV vs Ag/AgCl, see Fig. 4b).

In light of the possible structure of the acid base interactions of the surface oxide, it is critical to establish the nature of the oxygen species under cathodic disbond environments. The analysis is somewhat complicated by the presence of a large quantity of silicon that exists either as silica, SiO_2, or the highly hydrated and hydroxylated silica gel.

The typical O 1s XPS spectrum for the carbon steel sample treated in the 0.2% ammonium hydroxide consisted of two peaks at 532.4 and 530.2 eV respectively (see the "no heating" curve in Fig. 26). It was found previously that a high energy oxygen peak could be attributed to adsorbed water while lines at 531.1eV and 530.6eV correspond to hydroxyl and oxide oxygens respectively.[31,32] The low energy line at 530.2 eV can be attributed to Fe_3O_4. This result agrees with reports by Castle and Watts[3] and Hammond et al[5] who report 530.2 eV and 530.3 eV respectively for the iron oxide 1s spectrum from disbond zones of polymer coated steel. The samples for these experiments were not subject to a direct transfer from the environment to the UHV.

Since the high energy oxygen line at 532.4 eV can also be attributed to the oxygen of the silicon compound as well as the oxygen of adsorbed water, a series of experiments designed to distinguish these species was performed. Accordingly, the sample treated at -510 mV vs SCE was heated to different temperatures followed by XPS analysis. If the high energy oxygen exists as adsorbed water it would disappear with heating at relatively low temperatures. If, on the other hand, the high energy 1s O peak were due to silica, it would remain with heating.

The O 1s spectra obtained after a series of thermal treatments appear in Fig. 26. These results may be summarized in terms of line energies and integrated intensities (Figs. 27-32). The energies for the two lines show little shift until the sample is heated to 500°C at which point the low energy line shifted dramatically to 530.8 eV (Fig. 27). The the low energy line broadens while the high energy line narrows (Fig. 28). The total oxygen content decreases with the heating, showing a 25% decrease after heating at 500°C (Fig. 29). Initially the fraction of the high energy line increases at the expense of the fraction of the low energy line (Fig. 31). After heating at 500°C,

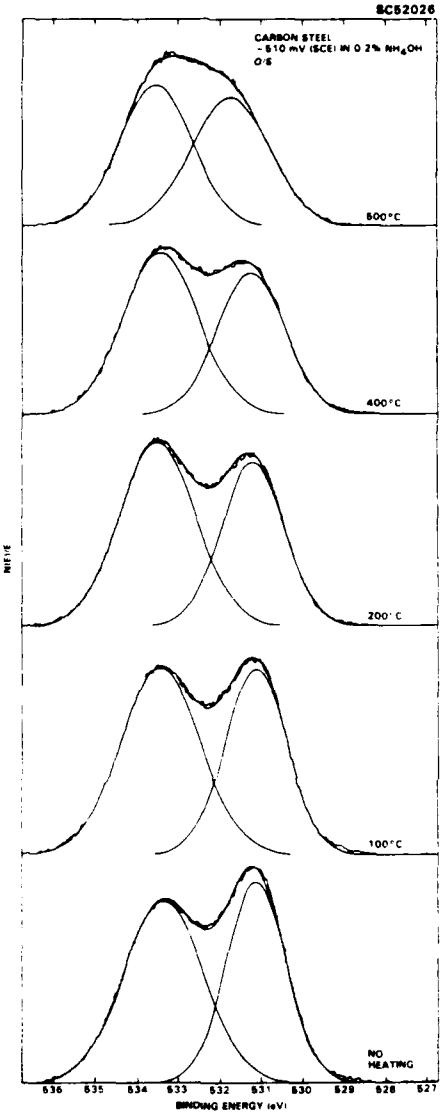

Fig. 26

O 1s XPS spectra for the carbon steel prepared at -510 mV vs SCE and then treated in vacuum ($< 10^{-9}$ torr) at the indicated temperatures.

the fraction of the low energy line increases (Fig. 30) and the iron is completely reduced to the metallic state. This is shown by the Fe 2p spectrum taken after heating as compared to the spectrum before heating (Fig. 31). The Si 2p spectra show no change with heating to 500°C (Fig. 32).

The oxygen spectrum and its behavior with heating of the sample is consistent with the following explanation. The low energy line at 530.2eV is for the oxygen of Fe_3O_4, while the high energy line is associated SiO_2. With heating the iron compound

Fig. 27

Peak energies determined from computer fit for the high energy and low energy oxygen peaks as a function of treatment temperature.

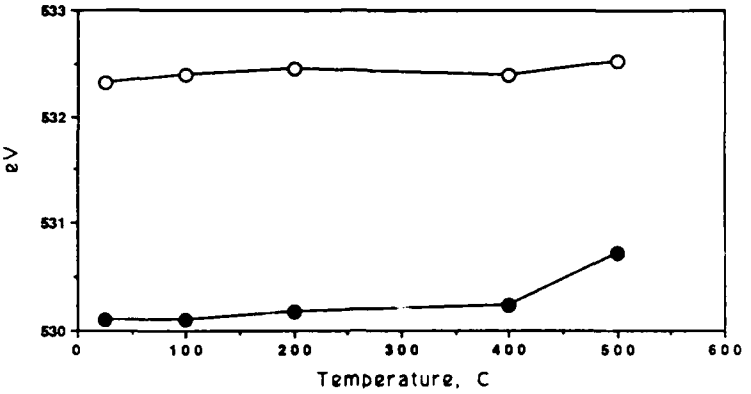

Fig. 28

Fitted line widths at half-maximum for the high energy (1) and low energy (2) O 1s XPS spectra as a function of treatment temperature.

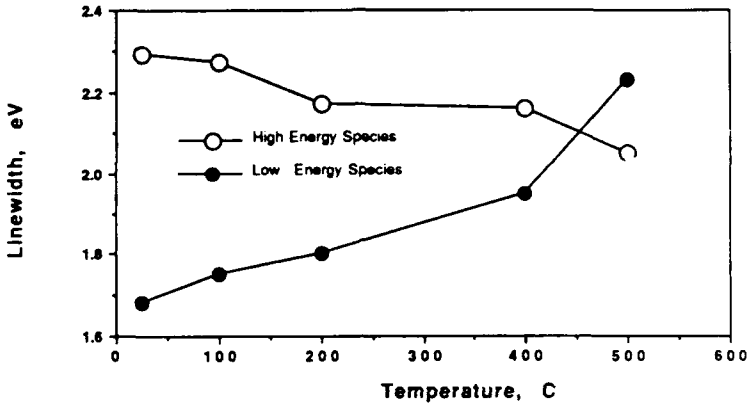

Fig. 29

Normalized integrated intensity for the O 1s spectrum as a function of the treatment temperature.

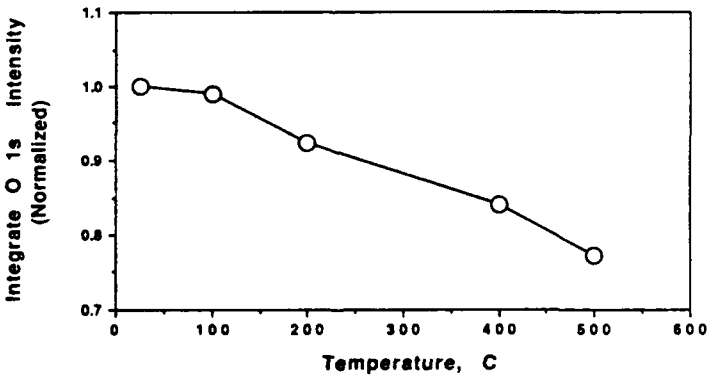

Fig. 30

Fraction of the high energy oxygen (1) and the low energy oxygen (2) as a function of the treatment temperature.

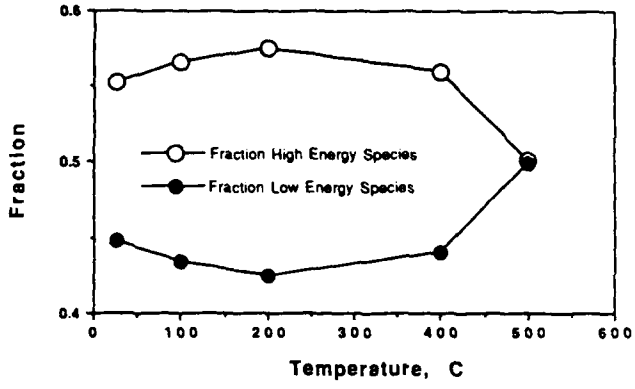

Fig. 31

Fe 2p spectra for carbon steel treated at -510 mV (SCE) in 0.2% NH_4OH and transferred to the UHV for XPS analysis. Spectra are taken before and after heating the sample.

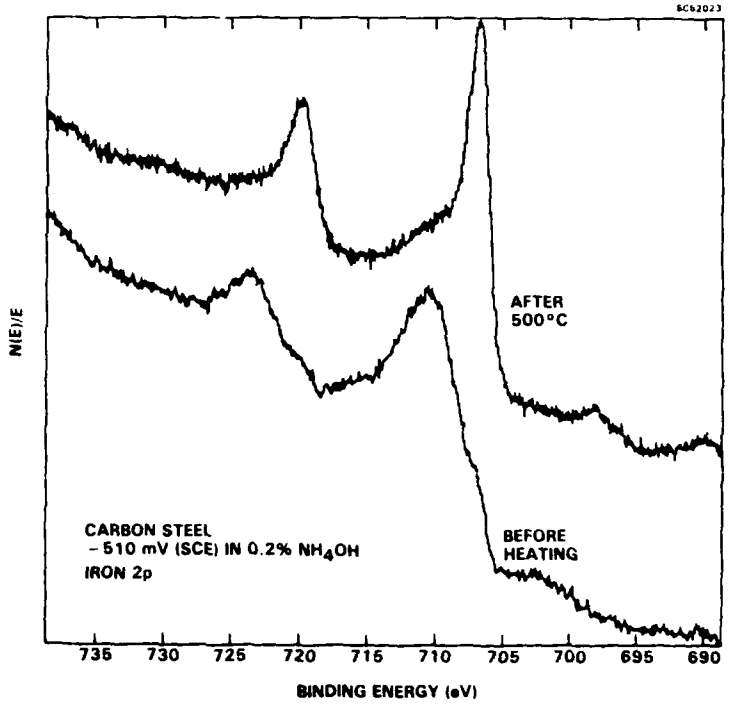

reduces with loss of water and oxygen and the low energy peak diminishes. For a sufficiently high temperature in vacuum (500°C), the low energy line actually disappears, the iron is entirely reduced. The new and broader low energy line at 530.8 eV has not been identified but is most likely associated with a silica compound.

The presence of silica on the sample surface represents an experimental artifact which is difficult to overcome for the alkaline environments of interest. It is

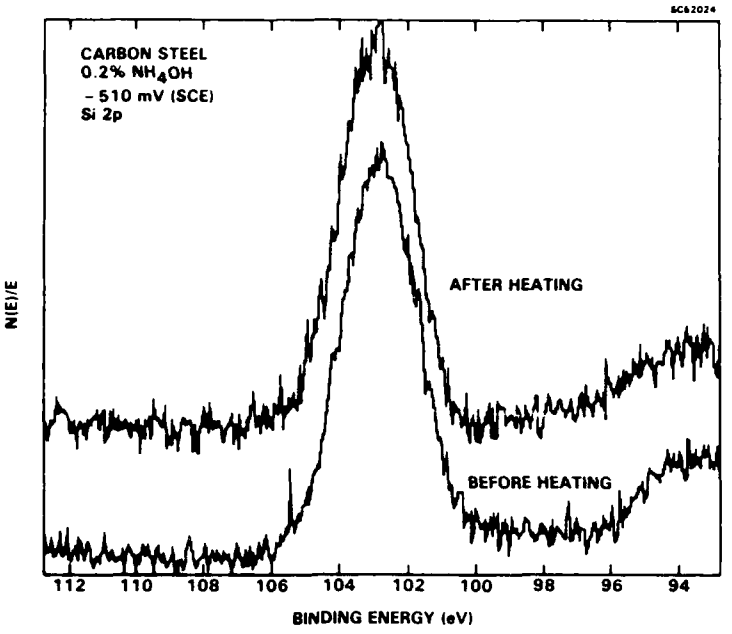

Fig. 32

Si 2p spectra for carbon steel treated at -510 mV (SCE) in 0.2% NH_4OH and transferred to the UHV for XPS analysis. Spectra are taken before and after heating the sample.

important to note that the adherence of the silica to the steel surface suggests a means for inhibiting cathodic disbonding. While this present work hardly demonstrates any beneficial influence of silica for inhibiting cathodic disbonding, silica does show a high affinity of the steel under alkaline conditions. With a sufficiently high concentration, a silica film may inhibit the cathodic reaction. Previous work at the Science Center has, in fact, provided some anecdotal evidence for the beneficial influence of silica for cathodic disbonding.[34] A high silicon concentration in the cathodic disbond zone might be achieved with a glass pigmented paint. Alkaline conditions at the coating metal interface would leach silicate from the glass pigment which could adsorb on the cathodic sites of the steel surface.

7.0 CONCLUSIONS AND RECOMMENDATIONS

Several important conclusions can be drawn from this work.

1. The generation of alkaline electrolyte at the coating steel interface irreversibly degrades the organic film (Fig. 3).

2. Alkaline electrolyte has a lower surface tension and, therefore, tends to displace organic films from the metallic surface (Figs. 7 and 9). Even in the absence of applied electrochemical potential (current) a cathodically generated quantity of base continues to drive the disbonding process (Fig. 4c).

3. The cathodic generation of a high pH electrolyte catalyzes the wetting of a rough surface as a result of the lowered surface energy of the electrolyte (Fig. 7, Fig. 9, Table 2).

4. Electrochemical transformation of the iron(III) oxide to a reduced state results in a rapid cathodic production of OH^- from the reduction of water and oxygen.

5. An oxalic acid/peroxide surface treatment renders carbon steel somewhat acidic as defined by Fowkes et al[28] (Fig. 15).

6. The surface of the steel under model cathodic disbonding conditions (0.2% NH_4OH) is Fe_3O_4 (Fig. 25). For potentials above -950 mV(SCE) the oxide is slightly oxidized. Below -1100 mV, the oxide becomes unstable with respect to the metal.

7. Sufficiently high cathodic polarization forces steel below the potential of zero charge which is about -550 mV vs Ag/AgCl in a pH 9.6 borate solution (Fig. 20-22). As a result the steel has a negative zeta potential and, therefore, repels organic layers with a zeta potential of the same polarity (Figs. 16-17).

8. Large molecular weight organic cations in organic films can stabilize the films against displacement from a cathodically polarized steel surface by an aqueous environment (Fig. 22).

A recommended approach for designing an organic coating for improved adhesion to steel under cathodic polarization is to graft a low concentration of fixed positively charged species onto the polymer backbone. Suitable inhibiting counter ions such as molybdate or borate could be used. This will give the coating a positive zeta potential and promote adhesion to cathodically polarized steel. This mechanism may, in fact, explain the enhanced corrosion resistance afforded by cathodically deposited organic coatings which most certainly would contain some residual positive charges.

Further investigation of the role of silicon oxides and hydroxides in promoting adhesion of organic coatings under cathodic conditions is recommended. This should be evaluated both from a fundamental standpoint as to whether or not silica or silica gel deposition inhibits cathodic reactions as well the more technological question of whether silica containing paints improve resistance to cathodic disbonding.

The results of this work demand some additional comments on the mechanism of cathodic disbonding of organic coatings from steel. Our results suggest that it is unlikely that oxide reduction represents the rate determining step in cathodic disbonding although oxide reduction may occur under some extreme conditions. The polymer desorption by molecular displacement of the polymer by water and hydroxide ion in the aqueous phase for potentials above the pzc (which may be as high as -550 mV depending on pH) initiates the process. This displacement should be reversible except when it occurs with sufficient cathodic polarization to generate large quantities sodium hydroxide that irreversibly degrade the polymer and lower the surface tension of the electrolyte. Indeed, significant disbonding of a coating occurs only at potentials significantly more negative (-750 mV vs Ag/AgCl) than the apparent pzc of -550 mV (pH 9.6). The alkaline degradation of the polymer renders the disbonding irreversible since the degraded polymer surface will no longer match the substrate to form an intimate molecular contact. In addition, the presence of a high pH electrolyte also inhibits reattachment of basic organic groups of the polymer to the acidic steel substrate (or alternatively acidic polymer groups from a basic steel surface depending on the polymer and surface pretreatment). Note that Leidheiser argues as we do here that the

substrate is acidic to the polymer base[39] while a phenolic polymer adhesive was considered in a recent report[40] to be acidic to the substrate base. In either case a high OH^- concentration will attack the coating-steel acid-base bond. The mechanism suggested by our work represents a combined interfacial failure[9,39,40] with subsequent polymer degradation.[6-8] The interfacial failure provides the primary step enabling cathodic reactions to proceed thereby generating a high pH for the polymer degradation which in turn renders the disbonding irreversible.

8.0 APPENDIX - DEFINITIONS AND EQUATIONS FOR SURFACE ENERGETICS[35,36]

Referring to Fig A-1, the wetting force F_w (total force minus that due to gravity and corrected for buoyancy) on the solid rod at the three phase boundry (defined by phases a, b, s) relates to the surface tension of the ab surface, γ_{ab}, by the equation:

$$F/P = \gamma_{ab} \cos \theta_{sab} = A_{sab} \tag{A-1}$$

$\gamma_{ab}\cos\theta_{ab}$ has been defined as the adhesion tension, A_{sab}.[37] For a sessile drop of liquid a on solid s, in the presence of a totally immiscible liquid b (see Fig. A-2), Young's equation can be generalized as

$$\gamma_{sb} = \gamma_{as} + \gamma_{ab} \cos \theta_{sab} \tag{A-2}$$

Assuming no solubility of any of the phases in each other, the respective works of adhesion can be written as

$$W_{ab} = \gamma_a + \gamma_b - \gamma_{ab} \tag{A-3}$$

$$W_{sa} = \gamma_s + \gamma_a - \gamma_{sa} \tag{A-4}$$

$$W_{sb} = \gamma_s + \gamma_b - \gamma_{sb} \tag{A-5}$$

rearranging the above equations allows A_{sab} to be related to the difference in the work of adhesion of the solid to the two respective liquid phases:

$$A_{sab} = \Delta W - \Delta \gamma \tag{A-6}$$

where

$$\Delta W = W_{sa} - W_{sb} \tag{A-7}$$

and

$$\Delta\gamma = \gamma_a - \gamma_b \qquad \text{(A-9)}$$

Here γ_a amd γ_b are the respective surface tensions of the liquid phases. For no solubility of a and b, $\Delta\gamma$ is a constant. Hence A_{sab} depends only on the differences between the works of adhesion of liquids a and b, respectively, for the solid.

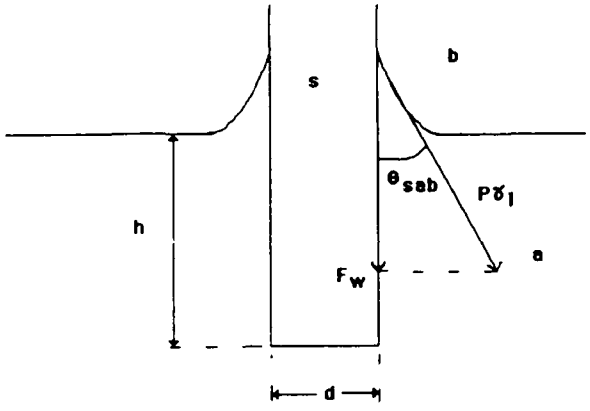

$$F_w = F_{total} - mg + 4\rho g/h\pi d^2$$

Wetting force = total force − gravitational force + buoyancy

Fig. A-1 Wetting forces on a cylindrical specimen.

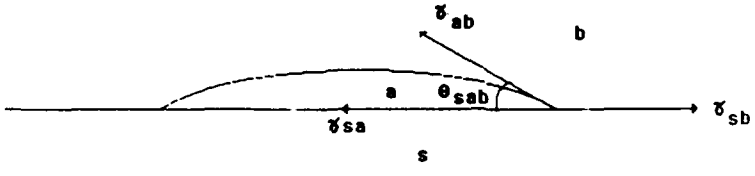

Fig. A-2 Sessile drop.

9.0 REFERENCES

1. G.W. Walter, Corros. Sci. 26(1), 27 (1986).

2. H. Gerhart, "Prophetic Imperatives in Corrosion Control," in 'Corrosion Control by Coatings,' H. Leidheiser, Jr.,ed., Science Press (1979).

3. M. Kendig and F. Mansfeld, "Lifetime Prediction of Organic coatings on Steel," Materials Research Society Proceedings 125 293 (1988).

4. J.E. Castle and J.F. Watts, Ind. Eng. Chem. Prod. R&D 24, 361 (1985).

5. J.W. Holubka, J.E. deVries and R.A. Dickie, Ind. Eng. Chem. Prod. Res. Dev. 23, 63 (1984).

6. J.S. Hammond, J.W. Holubka, J.E. DeVries and R.A. Dickie, Corrosion Sci. 21(3), 239 (1981).

7. J.W. Holubka and R.A. Dickie, J. Coat. Tech. 56(714), 43 (1984).

8. J.W. Holubka, J.S. Hammond, J.E. DeVries and R.A. Dickie, J. Coat. Technol. 52(670), 63 (1980).

9. E.L. Koehler, Corrosion, 40(1),5 (1984).

10. J. Ritter, J. Coatings Technol. 54, 695 (1982).

11. J.S. Thornton, R.E. Montgomery and J.F. Carter, "Failure Rate Model for Cathodic Delamination of Protective Coatings," NRL Memorandum Report, Contract No. N00014-83-C-2258 (1985).

12. R.C. Addison, Jr., M.W. Kendig and S.L. Jeanjaquet, "In situ Measurement of Cathodic Disbonding of Polybutadiene Coating on Steel," Acoustic Imaging, 17 (1988).

13. M. Kendig, R. Addison, and S. Jeanjaquet, "Environmental Integrity of Coating/Metal Interface," Annual Progress Report No. 1 for the Period February 1 through January 31, 1988, Contract No. N00014-87-C-0075, January 1988.

14. R.C. Addison, Jr., M.W. Kendig and S.L. Jeanjaquet, "Acoustic Microscopic Evaluation of Hydroxy-Terminated Polybutadiene on Steel," Proc. Ultrasonic Symposium of the IEEE, Chicago, 1988.

15. M. Kendig, R. Addison and S. Jeanjaquet, "Acoustic Microscopic Evaluation of Hydroxy-Terminated Polybutadiene on Steel," extended abstract, Proceedings of the 174th Meeting of the Electrochemical Society, October 1988.

16. M. Kendig, R. Addison and S. Jeanjaquet, "The Mechanism of Cathodic Disbonding of Hydroxy - Terminated Polybutadiene on Steel from Acoustic Microscopy and Surface Energy Analysis," extended abstract of a paper to be presented at Advances in Corrosion Protective Coatings, Cambridge, UK (April 1989).

17. M. Kendig and S. Jeanjaquet, "The Mechanism of Cathodic Disbonding of Hydroxy-Terminated Polybutadiene on Steel from Acoustic Microscopy and Surface Energy Analysis," in 'Proceedings of the Cambridge Symposium on Advances in Corrosion Protection by Organic Coatings,' PV-89-13, 1989, Electrochemical Society, Pennington, NJ.

18. H. Leidheiser, W. Wang, L. Igetoft, Progr. Org. Coatings 11, 19 (1983).

19. M. Cohen, "The Passivity and Breakdown of Passivity on Iron," in 'Passivity of Metals,' edited by R. Frankenthal and J. Kruger, Corrosion Monograph Series, Electrochemical Soc., 1978.

20. J.B. Lumsden and P.J. Stocker, "Effect of Transfer Technique Between Solution and UHV on the Chemistry of Passive Films on Well-Defined Stainless Steel Surfaces," in Passivity of Metals and Semiconductors,' M. Froment, ed., Elsevier (1983).

21. M. Kendig, "Environmental Integrity of Coating/Metal Interface," Annual Progress Report for the Period February 1, 1988 through January 31, 1989.

22. B. Boukamp, "EQUIVCRT," University of Twente, P.O. Box 217, 7500 Enschede, Netherlands, 1988, and B. Boukamp, in 'Computer Aided Acquisition and Analysis of Corrosion Data,' M. Kendig ed., PV 85-3, Electrochemical Society Proceedings Volume, 1985.

23. M. Kendig, E. Meyer, G. Lindberg, and F. Mansfeld, Corros. Sci. 23(9), 1007 (1983).

24. R.N. Wenzel, Ind. Eng. Chem. 28, 988 (1936).

25. R. Shuttleworth and G. Bailey, Disc. Faraday Soc. 3, 16 (1948).

26. R. Dettre and R. Johnson, Adv. Chem. Ser., No. 43, 112 (1963).

27. O. Teschke, M.U. Kleinke, M.A. Tennan, J. Electrochem. Soc. 137(3), 781 (1990).

28. F. Fowkes and M. Mostafa, Ind Eng. Chem. Prod. R&D 17(1), 1978. See also R. Drago, L. Parr, J. Am., Chem. Soc. 99(10), 3203 (1982).

29. J.C. Bolger and A.S. Michaels, "Molecular Structure and Electrostatic Interactions at Polymer-Solid Interfaces," in 'Interface Conversion for Polymer Coatings,' P. Weiss, G. Cheever, eds., Elsevier, 1968.

30. G.F. Brewer, "Corrosion Resistance of Paint Films from andodic and Cathodic Resins," in 'Corrosion Control by Coatings,' H. Leidheiser, Jr., ed., Science Press (1979).

31. N.S. McIntyre and G. Zetaruk, Anal. Chem. 49, 1521 (1977).

32. J. Lumsden and P. Stocker, "Characterization of Passive Films formed on Stainless Steel in High Temperature Water," in 'Passivity of Metals and Semiconductors,' M. Froment, ed., Elsevier, 579, 1983.

33. Miller and Linton, Anal Chem. 57, 2314 (1985).

34. M. Kendig, S. Tsai and F. Mansfeld, Materials Performance 23(6), 37 (1984).

35. A.W. Adamson, "Physical Chemistry of Surfaces," 4th edition, John Wiley, 1982.

36. R. Aveyard and D.A. Haydon, "An Introduction to the Principles of Surface Chemistry," Cambridge Chemistry Texts, Cambridge, 1973.

37. F.E. Bartell, L.S. Bartell, J. Am. Chem. Soc. 56(11), 2205 (1934).

38. V. Agarwala, "Multipurpose Corrosion Inhibitors for Aerospace Alloys in Naval Environments," in New Materials and New Processes, JEC Press, Cleveland, OH, Vol. 3, p 178, 1985.

39. H. Leidkeiser, J. Adhesion Sci. Tech. 1(1), 79 (1987).

40. R. Hamadek, "An Interdisciplinary Study of Cathodic Disbonding in Elastomer/Metal Adhesive Bonds," Final Report, Virginia Tech Center for Adhesive and Sealant Science, Contract No. N00014-85-K-0145-P00003, October 1988.